Edinburgh Research Explorer

Strongly truncated Dnaaf4 plays a conserved role in Drosophila ciliary dynein assembly as part of an R2TP-like co-chaperone complex with Dnaaf6

Strongly truncated *Dnaaf4* plays a conserved role in *Drosophila* ciliary dynein assembly as part of an R2TP-like co-chaperone complex with *Dnaaf6*

1   **Jennifer Lennon[1,3][†], Petra zur Lage[1][†], Alex von Kriegsheim[2][*], Andrew P. Jarman[1,][***]**
2
3   [1]Centre for Discovery Brain Sciences, Edinburgh Medical School, University of Edinburgh,
4   Edinburgh, UK EH8 9XD, UK
5   [2]Edinburgh Cancer Research UK Centre, Institute of Genetics and Cancer, University of Edinburgh,
6   Edinburgh, EH4 2XU, UK
7   [†]These authors share first authorship

8   *** Correspondence:**
9   Dr Andrew Jarman
10 andrew.jarman@ed.ac.uk

11 [3]Current address: Department of Biology, New York University, 100 Washington Square East, New
12 York, NY 10003, USA

14

15 **Abstract**
16 Axonemal dynein motors are large multi-subunit complexes that drive ciliary movement.
17 Cytoplasmic assembly of these motor complexes involves several co-chaperones, some of which are
18 related to the R2TP co-chaperone complex. Mutations of these genes in humans cause the motile
19 ciliopathy, Primary Ciliary Dyskinesia (PCD), but their different roles are not completely known.
20 Two such dynein (axonemal) assembly factors (DNAAFs) that are thought to function together in an
21 R2TP-like complex are DNAAF4 (DYX1C1) and DNAAF6 (PIH1D3). Here we investigate the
22 *Drosophila* homologues, *CG14921/Dnaaf4* and *CG5048/Dnaaf6*. Surprisingly, *Drosophila* Dnaaf4 is
23 truncated such that it completely lacks a TPR domain, which in human DNAAF4 is likely required to
24 recruit HSP90. Despite this, we provide evidence that *Drosophila* Dnaaf4 and Dnaaf6 proteins can
25 associate in an R2TP-like complex that has a conserved role on dynein assembly. Both are
26 specifically expressed and required during the development of the two *Drosophila* cell types with
27 motile cilia: mechanosensory chordotonal neurons and sperm. Flies that lack *Dnaaf4* or *Dnaaf6*
28 genes are viable but with impaired chordotonal neuron function and lack motile sperm. We provide
29 molecular evidence that *Dnaaf4* and *Dnaaf6* are required for assembly of outer dynein arms (ODAs)
30 and a subset of inner dynein arms (IDAs).

1   INTRODUCTION
32
33 Ciliary motility is driven by a highly conserved family of axonemal dynein motors, which are large
34 multi-subunit complexes (King, 2016). Those that comprise the Outer Dynein Arms (ODA) are the
35 main drivers of motility, whereas those of the Inner Dynein Arms (IDA) modulate ciliary movement.
36 During ciliogenesis, the assembly of the motors into the cilium or flagellum is highly regulated. After
37 subunit synthesis, complex assembly occurs within the cytoplasm (known as pre-assembly) prior to
38 transport and docking within the cilium (Fok et al., 1994; Fowkes and Mitchell, 1998). This pre-
39 assembly is facilitated by a series of regulators called dynein pre-assembly factors (DNAAFs) (King,

40 2016). Many of these factors were originally identified as causative genes of human Primary Ciliary
41 Dyskinesia (PCD), but they are highly conserved among eukaryotes that have motile ciliated cells
42 (Omran et al., 2008). This conservation was recently shown to be true for *Drosophila melanogaster*,
43 which has an almost full complement of homologous genes for the axonemal dynein complexes and
44 for dynein assembly factors (zur Lage et al., 2019). In the case of *Drosophila*, ciliary motility is
45 confined to the sensory cilium of mechanosensory neurons (chordotonal neurons) and the sperm
46 flagellum. Flies with dysfunctional dyneins are therefore deaf, uncoordinated and have immotile
47 sperm, which makes the fly a convenient model for analysis of motile ciliogenesis (Diggle et al.,
48 2014; Moore et al., 2013; zur Lage et al., 2018; zur Lage et al., 2021).

49

50 The specific functions of DNAAFs are beginning to be unravelled, and in many cases they are
51 thought to function as co-chaperones that regulate HSP70/90 to facilitate correct folding of the
52 dynein heavy chains as well as subunit assembly (Fabczak and Osinka, 2019). Chaperones are
53 important for many cellular functions including the assembly of large multi-subunit complexes like
54 axonemal dynein motors. For several DNAAFs, such a function is strongly indicated by DNAAF
55 sequence relationships with a known HSP90 co-chaperone, the R2TP complex (Maurizy et al., 2018).
56 This co-chaperone was discovered in *S. cerevisiae* as facilitating RNA polymerase II assembly (Zhao
57 et al., 2005). In humans, R2TP comprises the ATPases RUVBL1 and RUVBL2, a TPR
58 (tetratricopeptide repeat) protein RPAP3, and a Pih domain protein PIH1D1 (Table 1). R2TP
59 facilitates the assembly/stabilisation of several multi-subunit complexes, including RNA polymerase
60 II, PIKKs (Houry et al., 2018; Kakihara and Houry, 2012). Much is known of the structural features
61 of R2TP: for RPAP3, the TPR domains directly recruit HSP70 and HSP90 while the RPAP3_C
62 domain binds to RUVBL2 (Martino et al., 2018). For PIH1D1, the PIH domain recruits client
63 proteins, while the CS domain binds to a region of RPAP3 C-terminal to the TPR domain (Kakihara
64 and Houry, 2012; Martino et al., 2018; Maurizy et al., 2018).

65

66 **Table 1 Genes referred to in this study**

67

Drosophila	Flybase ID	Human*	*C. reinhardtii*	Danio rerio
pontin (pont)	FBgn0040078	*RUVBL1*	*CrRuvBL1*	*ruvbl1*
reptin (rept)	FBgn0040075	*RUVBL2*	*CrRuvBL2*	*ruvbl2*
spaghetti/Rpap3	FBgn0015544	*RPAP3*	*Cr02.g084900*	*rpap3*
Spag1	FBgn0039463	*SPAG1*	*Spag1*	*spag1a/b*
CG14921/Dnaaf4	FBgn0032345	*DNAAF4 (DYX1C1)*	*pf23/DYX1C1*	*dnaaf4*
Pih1D1	FBgn0032455	*PIH1D1*	*mot48?*	*pih1d1*
CG4022/Pih1D2	FBgn0035986	*PIH1D2*	*n/a*	*pih1d2*
CG5048/Dnaaf6	FBgn0036437	*DNAAF6 (PIH1D3)*	*twi(?)*	*twister*
Nop17l	FBgn0033224	*DNAAF2/KTU*	*pf13*	*ktu*
Heatr2/Dnaaf5	FBgn0051320	*DNAAF5/HEATR2*	*htr2*	*heatr2*

68 *Following nomenclature recommendations in Braschi et al. (Braschi et al., 2022).

69

70 There is evidence that mutation of Ruvbl1/2 also causes ciliary dynein defects (Li et al., 2017; Zhao
71 et al., 2013). While this may partly be due to involvement of R2TP in dynein pre-assembly as has
72 been demonstrated in *Chlamydomonas*, zebrafish and *Drosophila* (Liu et al., 2019; Yamaguchi et al.,
73 2018; zur Lage et al., 2018), it is thought that Ruvbl1/2 may also function with DNAAFs to form
74 'R2TP-like' complexes specifically required for dynein assembly (Fig. 1A) (Olcese et al., 2017; Pal
75 et al., 2014; Vaughan, 2014). Among the DNAAFs, SPAG1 has both TPR and RPAP3_C domains,
76 while DNAAF4 (DYX1C1) has TPR and CS domains. Similarly, the CS and PIH domains of

77   PIH1D1 are also present in several other PIH proteins: PIH1D2, DNAAF2 (KTU), and DNAAF6
78   (PIH1D3) (Dong et al., 2014). There is biochemical evidence that SPAG1 complexes with PIH1D2
79   and DNAAF2 (Maurizy et al., 2018; Smith et al., 2022). Different isoforms of DNAAF4 complex
80   with DNAAF2 and DNAAF6 (Maurizy et al., 2018; Olcese et al., 2017; Paff et al., 2017; Tarkar et
81   al., 2013). However, while these are also referred to as R2TP-like complexes (Olcese et al., 2017), it
82   is not clear whether Ruvbl1/2 (i.e. R2) are involved, particularly as DNAAF4 lacks an RPAP3_C
83   domain. Whether these putative complexes function *in vivo* and their precise role during dynein
84   assembly are not fully established, but they may be required for different steps in the process or for
85   the assembly of different dynein subtypes.
86
87   For the PIH proteins, the possibility of different roles during dynein assembly has been raised by
88   experiments in zebrafish and *Chlamydomonas* (Yamaguchi et al., 2018; Yamamoto et al., 2010;
89   Yamamoto et al., 2020). In zebrafish, *pih1d1*, *pih1d2* and *ktu* and *twister* (DNAAF6 homologue)
90   have overlapping functions in the assembly of ODAs and IDA subsets based on analyses of mutant
91   spermatozoa (Yamaguchi et al., 2018). Similarly, in a proteomic profiling of *Chlamydomonas*
92   mutants, *mot48* (PIH1D1) *pf13* (DNAAF2) and *twi* (DNAAF6) have overlapping but distinct roles in
93   assembly of dynein complex subsets (Yamamoto et al., 2010; Yamamoto et al., 2020).
94
95   Of the TPR-containing DNAAFs, *DNAAF4* is a cause of PCD in humans, with motile cilia showing
96   reduction in subsets of ODAs and IDAs (Tarkar et al., 2013). In *Chlamydomonas* the DNAAF4
97   homologue also shows a partial reduction in ODAs and some IDAs (Yamamoto et al., 2017). In
98   addition to this ciliary motility role, DNAAF4 was originally identified (as DYX1C1) as being
99   affected by a chromosomal translocation associated with susceptibility to developmental dyslexia
100 (Taipale et al., 2003), and subsequently a role for this gene in cortical neuron migration was proposed
101 (Wang et al., 2006). Neither function has an obvious direct link to ciliary motility, suggesting that
102 DNAAF4 may have wider roles beyond dynein pre-assembly. Similarly, SPAG1 may have roles in
103 addition to dynein pre-assembly: R2SP complexes with PIH1D2 were characterised in cells that lack
104 motile cilia (Chagot et al., 2019; Maurizy et al., 2018), and a constitutively expressed isoform exists
105 (Horani et al., 2018). Interestingly, mice homozygous for a null allele of *Dnaaf2* do not progress
106 beyond stage E9.5, and have multiple pathologies that are difficult to ascribe to failure of ciliary
107 motility alone (Cheong et al., 2019).
108
109 Thus, the roles of TPR- and PIH-domain containing DNAAFs in assembling subsets of dynein
110 complexes remain to be fully disentangled, as do the identities of the R2TP-like complexes that
111 function in vivo. Moreover, the question of functions for TPR subunits (and by extension the
112 complexes) beyond dynein assembly also remains open.
113
114 We have previously shown that *Drosophila* has homologues of *SPAG1* and *DNAAF4* (zur Lage et al.,
115 2019) (Table 1), and that *Drosophila* Spag1 is required for dynein assembly and is able to form a
116 complex with Ruvbl1/2 and Pih1d1 (zur Lage et al., 2018). However, the predicted Dnaaf4 protein is
117 truncated such that it lacks any TPR domain, bringing into question its ability to function in a co-
118 chaperone complex. *Drosophila* has homologues of all the PIH proteins (zur Lage et al., 2019). Most
119 *Drosophila* PIH genes appear widely expressed, but *Dnaaf6* expression appears to be restricted to
120 motile cilia cells. Here we characterise the function of *Drosophila Dnaaf4* and *Dnaaf6* as potential
121 R2TP-like partners. Despite the truncation of Dnaaf4, we show that Dnaaf4 and Dnaaf6 proteins can
122 form an R2TP-like complex, and that each is required for assembly of ODAs and a subset of IDAs.
123 Moreover, there is no indication of functions other than dynein assembly.

124 **2   MATERIALS AND METHODS**

2.1   Fly stocks

Fly stocks were maintained on standard media at 25°C. The following UAS RNAi stocks were obtained from the Vienna *Drosophila* Resource Center (Dietzl et al., 2007): KK60100 (genetic background stock used as negative control) KK111069 (*Dnaaf4*), KK108561 (*Dnaaf6*) and KK100470 (*Spag1*). The following were obtained from the Bloomington Drosophila Stock Centre: Or-R as wild-type control (#2376), UAS-*Dcr2* (#24644), w^{1118} y^1 M{vas-Cas9} ZH-2A/FM7c (#51323), y^1 w^* $P\{y^{t7.7}=nos$-phiC31\int.NLS}X; $P\{y^{t7.7}=CaryP\}attP40$ (#79604) and w^*; P{UASp-Venus.GAP43}7 (#30897). Dnali1-mVenus, Dnal1-mVenus are described in Xiang et al. (Xiang et al., 2022). Flies with UAS-int attp40 landing site were obtained from the Cambridge Microinjection facility. The *sca-Gal4* line used for sensory neuron knockdown was a gift from M. Mlodzik (Baker et al., 1996) and was used in conjunction with UAS-*Dcr2*. For male germline knockdown, *w; Tft/CyO; Bam-Gal4*-VP16 was a gift from Helen White-Cooper.

2.2   Sequence analyses

For detecting orthology, DIOPT was used (Hu et al., 2011). For phylogenetic analysis, protein sequences were obtained from BLAST, Uniprot (Bateman et al., 2021) and Flybase (Larkin et al., 2021). Sequences were aligned using CLUSTALW/MUSCLE within MEGA7 (Kumar et al., 2016). Tree analysis was conducted using the Maximum Likelihood method within MEGA7.

2.3   In situ hybridisation on whole-mount embryos

Primers were designed to give a probe of around 420-bp with the reverse primer containing the T7 RNA polymerase promoter at its 5' end (all primers are in Supplementary Table S1). DNA was amplified from genomic DNA by PCR and then DIG-labelled RNA generated (DIG RNA Labelling Mix, Roche Cat. No.11277073910) using T7 RNA polymerase (Roche Cat. No. 10881767001). RNA in situ hybridisation was carried out according to zur Lage et al. (2019). In the case of RNA in situ/antibody staining double labelling, antibody staining was carried out after the ISH had been developed. Images were taken on an Olympus AX70 upright microscope with DIC optics.

2.4   Immunofluorescence

Immunohistochemistry on embryos and pupal antenna was described in zur Lage et al. (zur Lage et al., 2018). *Drosophila* testis fixing and staining was carried out according to Sitaram et al. (Sitaram et al., 2014). The following primary antibodies were used: goat anti-GFP antibody (1:500, ab6673), rabbit anti-GFP antibody (1:500, Life Technologies, A11122), mouse anti-Futsch antibody (1:200, Developmental Studies Hybridoma Bank, 22C10), mouse anti-pan polyglycylated tubulin (1:100, Merck, MABS276), rabbit anti-Sas-4 (1:350, gift from Jordan Raff) and rabbit anti-Dnah5 antibody (1:2000, (zur Lage et al., 2021)). The following secondary antibodies were used: goat anti-Rabbit antibody (1:500, Alexa Fluor 488, Life Technologies, A11008) and goat anti-Mouse antibody (1:500, Alexa Fluor 568, Life Technologies, A11019), donkey anti-goat antibody (1:500, Alexa Fluor 488, Life Technologies, A11055), donkey anti-mouse antibody (1:500, Alexa Fluor 568, Life Technologies, A10037), and donkey anti-rabbit antibody (1:500, Alexa Fluor 647, Life Technologies, A31573). Phalloidin was used 1:2000 (Life Technologies, A12380). DNA in adult testes was stained with To-Pro-3 (1:1000, Life Technologies, T3605) or DAPI (14.3mM, Life Technologies) solution in the dark for 15min. After several washes, the samples were mounted on slides with 85% glycerol and 2.5% propyl gallate (Sigma, P3130). Images were captured using a Zeiss LSM-5 PASCAL/Axioskop 2 and a Leica TCS SP8 confocal microscope and processed with Fiji.

2.5   mVenus fusion gene construction

mVenus fusion genes were constructed for Dnaaf4 and Dnaaf6 by amplifying gene segments from genomic DNA and cloning into pDONR221 using the BP clonase II from Gateway technology (Thermo Fisher Scientific). The segment included introns, 5' UTR, TSS, and additional upstream flanking DNA of approximately 1 kb, but lacked the stop codon. The insert was subsequently transferred to the destination vector pBID-GV (modified from pBID-UASC-GV vector (Wang et al. 2012) where the UASC had been deleted) with the help of LR clonase II (Gateway technology, Thermo Fisher Scientific). This put the ORF in-frame with the mVenus coding sequence. Transformant fly lines were generated by microinjection into syncytial blastoderm embryos of the attP40 landing site line.

2.6   *Dnaaf4* and *Dnaaf6* CRISPR/Cas9 mutant construction

The CRISPR/Cas9 mutant lines were designed by substituting the coding regions of the gene with the mini-white gene. CRISPR primers were designed using the flyCRISPR OptimalTarget finder programme. The cloning was performed according to Vieillard et al. (Vieillard et al., 2016) and injection into the Cas9 line was carried out by the *Drosophila* Microinjection Services (Department of Genetics, Cambridge, UK).

2.7   Fertility, hearing and climbing assays

These assays were carried out as described in zur Lage et al. (2021). In the fertility assay, individual males were crossed to pairs of virgin OrR females and resulting progeny counted. For climbing assays, 2-5 day-old adult females were tested in batches of 15. For the larval hearing assay, batches of 5 third instar larvae on an agar plate placed on a speaker were tested for response to a 1000-Hz tone. *n* for each genotype = 5 batches of 5 larvae, each exposed to 3 tones 30 s apart. For visual analysis of spermatogenesis, testes were dissected, mounted in PBS, and then observed immediately by DIC optics.

2.8   Protein expression analysis of testes by MS

Knockdown males were generated by crossing UAS-RNAi males from *Dnaaf4*, *Spag1* and the KK control line to *Bam*-Gal4 at 25ºC. 1-3 days post-eclosion male progeny were dissected in ice-cold PBS and 30 pairs of testes with four replicates per genotype were snap-frozen in liquid nitrogen before subsequently being processed and analysed for label-free mass-spectrometry as described in zur Lage et al. (2018). The mass spectrometry proteomics data have been deposited in the ProteomeXchange Consortium via the PRIDE (Perez-Riverol et al., 2019) partner repository with the dataset identifier PXD033608.

2.9   Transmission electron microscopy (TEM)

Adult heads were cut off and the proboscis was removed to facilitate infiltration of the solution. The head were rinsed in 0.1 M phosphate buffer before fixing overnight at 4°C in freshly made 2.5% glutaraldehyde, 2% paraformaldehyde in 0.1M phosphate buffer (pH 7.4) solution. Subsequently the samples were rinsed four times and then washed three times for 20min in 0.1M phosphate buffer at room temperature. Further processing for TEM, post-fixing and imaging was carried by Tracey Davey at the Electron Microscopy Research Services, Newcastle University Medical School, using a Philips CM100 CompuStage (FEI) microscope and an AMT CCD camera.

2.10   Transfection and coIP of S2 cells

208 RNA was prepared from *Drosophila* antennae or testes and mouse testes with the RNeasy Mini kit
209 (Qiagen 74106). cDNA was synthesised, the open reading frames were PCR amplified and
210 initially cloned into the pDONR221 plasmid using the BP clonase II of the Gateway system
211 (Life Technology) before transferring the fragments using the LR clonase II to the C-terminal
212 site of the destination plasmids pAWH (3xHA epitopes) and pAWF (3x FLAG epitopes) of the
213 *Drosophila* Gateway Vector collection (Carnegie Institution for Science). Primers for synthesis are
214 listed in Table S1. The truncated mouse Dyx1c1DTPR protein contains the first 227 amino acids of
215 the wildtype 420 amino acid protein, therefore omitting the whole of the C-terminal TPR domain and
216 replacing it with a stop codon. Transfection into S2 cells was performed according to the X-TREME
217 GENE HP DNA transfection reagent (Merck) protocol. After 48-72 h cells were harvested and coIP
218 was carried out according to the FLAG Immunoprecipitation kit (Sigma-Aldrich). Samples were run
219 on pre-cast gels (Bio-Rad) followed by Western blotting. The blots were then probed with mouse
220 anti-FlagM2 (1:1,000; F1804; Sigma-Aldrich) and rabbit anti-HA (1:4,000; ab9110; Abcam)
221 antibodies, followed by Li-COR secondary antibodies (IR Dye 680RD and IR Dye 800CW), before
222 protein detection on a Li-COR Odyssey scanner using Image Studio v5.2 software.

223 **2.11 GFP trap affinity purification and mass spectrometry**

224 150 pairs of testes in 3 replicates were dissected in ice-cold PBS for Dnaaf4-mVenus and control line
225 UAS-GAP43-mVenus x Bam-Gal4). The samples were snap-frozen in liquid nitrogen. Lysis buffer
226 (Tris-HCl pH7.5 50mM, NaCl 100mM, Glycerol 10%, EDTA 5mM, sodium deoxycholate 0.5%,
227 Complete Mini protease inhibitor) was added to samples before they were homogenised on ice for 2
228 minutes. Samples were subsequently rotated, incubated in a lysis buffer for 30 minutes at 4°c, and
229 then centrifuged, before being processed and analysed as described in zur Lage et al. (2018) with
230 following alterations: the data was acquired using a Fusion Lumos mass spectrometer (Thermo
231 Fisher) that was operated in an OT-IT configuration. 1-s cycle time, 120k resolution in the orbitrap
232 for MS and rapid scanning MS/MS in the ion-trap. Collision energy was set to 30.

233 **3   RESULTS**

234 **3.1   *Drosophila* has orthologues of DNAAF4 and DNAAF6, but the former is strongly
235   truncated thereby lacking a TPR domain**

236 Of the PIH genes in *Drosophila*, the orthology prediction tool DIOPT (Hu et al., 2011) identifies the
237 orthologue of *DNAAF6* as *CG5048* (hereafter named *Dnaaf6*). Predicted *Drosophila* Dnaaf6 protein
238 retains PIH and CS domains, and has 45% similarity and 30% identity with the human protein (Fig.
239 1B). For *DNAAF4*, DIOPT identifies the gene *CG14921* as the *Drosophila* orthologue. However, the
240 encoded protein of this gene (named *Dnaaf4*) is severely truncated relative to the human protein such
241 that it lacks the C-terminal TPR domain (Fig. 1B). Despite this, DIOPT predicts clear orthology with
242 human DNAAF4 for the remaining protein, with 40% similarity and 25% identity. Moreover, the
243 region of alignment is not limited to the CS domain (Supplementary Fig. S1). Phylogenetic analysis
244 indicates that this truncation occurred during dipteran evolution, as the truncation is shared by other
245 higher dipterans (Brachycera) but not lower dipterans or other insects (Fig. 1C). Interestingly, the
246 DNAAF4 sequences of brachyceran flies form a distinct group in a phylogenetic tree, even if just the
247 CS domains are compared (Fig. 1D). This suggests significant sequence divergence occurred in these
248 truncated *Dnaaf4* genes compared with the archetypal full-length genes present from single celled
249 algae to vertebrates.
250
251 Human DNAAF4 binds to HSP90 (Tarkar et al., 2013) and this is predicted to occur via its TPR
252 domain (Haslbeck et al., 2013). The loss of this domain in *Drosophila* Dnaaf4 may therefore be

253 expected to have profound consequences for the conservation of *Drosophila Dnaaf4* function as an
254 R2TP-like chaperone in dynein assembly. Below, this is explored by examining expression, protein
255 interactions and gene function.

3.2 *Drosophila Dnaaf4* and *Dnaaf6* are expressed exclusively in differentiating motile ciliated cells

258 Transcription of both *Dnaaf4* and *Dnaaf6* is highly specific to tissues with motile ciliated cells.
259 Examination of FlyAtlas 2 transcriptome data (Krause et al., 2022) indicates that *Dnaaf4* is expressed
260 specifically in adult testis. In addition, *Dnaaf4* is 5.2-fold enriched in the transcriptome of developing
261 embryonic chordotonal cells (zur Lage et al., 2019). *Dnaaf6* is also very highly expressed in testis,
262 and found to be enriched in chordotonal cells (55.4-fold). RNA *in situ* hybridisation confirms that
263 embryonic expression of each gene is confined to differentiating chordotonal neurons (Fig. 2A,C,E).
264 In *Dnaaf4* (but not *Dnaaf6*) this expression becomes restricted to a subset of lch5 neurons late in
265 differentiation (Fig. 2B). Expression of *Dnaaf6* was abolished in embryos homozygous for a
266 mutation in *fd3F*, which encodes a transcription factor that regulates motile ciliary genes (Newton et
267 al., 2012) (Fig. 2D).
268
269 Expression was confirmed in flies with mVenus fusion transgenes, each including about 1-kb of
270 upstream flanking sequence to drive expression under endogenous regulation (Fig. 2F). In each
271 reporter, there are predicted binding sites very close to the transcription start site for the cilia-
272 associated transcription factors fd3F and Rfx (marked F and X in the schematic, Fig. 2F), an
273 arrangement that has been noted for many other motile cilia genes (Diggle et al., 2014; Moore et al.,
274 2013; Newton et al., 2012; zur Lage et al., 2018). For both *Dnaaf4* and *Dnaaf6*, fusion protein was
275 detected in embryonic chordotonal neurons (Fig. 2G,H), the differentiating chordotonal neurons of
276 Johnston's organ (JO) in the pupal antenna (Fig. 2I,J), and also in developing spermatocytes (Fig.
277 2K,L). The fusion protein was located in the cytoplasm of these cells, consistent with a dynein pre-
278 assembly role.
279
280 In conclusion, despite the truncated nature of Dnaaf4, both proteins are expressed exclusively in
281 motile ciliated cells, consistent with a conserved function in motile ciliogenesis.

3.3 *Drosophila* Dnaaf4 and Dnaaf6 can associate in an R2TP-like complex

283 Protein interactions were explored by heterologous expression of tagged proteins in S2 cultured cells.
284 Firstly, for comparison we investigated the interactions of mouse Dnaaf4 and Dnaaf6 with each other
285 and with the *Drosophila* homologues of Hsp90, Ruvbl1 and Ruvbl2 (known as Pontin and Reptin in
286 *Drosophila*). The mouse homologues have an almost identical length and domain structure to the
287 human proteins shown in Fig. 1B. Coimmunoprecipitation confirmed that full-length mouse Dnaaf4
288 and Dnaaf6 can participate in an R2TP-like complex that also includes Hsp90 (Fig. 3A,B).
289 Interestingly, these results suggest that Pontin and Reptin can form part of such Dnaaf4/6 complexes
290 despite Dnaaf4's lack of RPAP3_C domain. We cannot exclude, however, that endogenous
291 (untagged) proteins participate in the detected complexes, thereby facilitating or bridging these
292 interactions.
293
294 We then investigated the *Drosophila* orthologues. *Drosophila* Dnaaf4 is able to complex with
295 *Drosophila* Dnaaf6, although this interaction appears to be weaker than that between the equivalent
296 mouse proteins (Fig. 3C). Given this association, we asked whether a truncated version of mouse
297 Dnaaf4 retains binding potential. However, this version (mDnaaf4ΔTPR) showed very poor ability to

298   bind to mouse Dnaaf6 (Fig. 3D). Interestingly each *Drosophila* protein is also able to complex with
299   Reptin/Pontin (Fig. 3E). As above, this could indicate a direct protein interaction, but it is also
300   possible that endogenous proteins facilitate these interactions. Either way, *Drosophila* Dnaaf4 and
301   Dnaaf6 can participate in complexes with Pontin and Reptin.
302
303   The lack of TPR domain in *Drosophila* Dnaaf4 implies that it is not able to recruit Hsp90. Indeed, we
304   found that *Drosophila* Dnaaf4 could not complex with Hsp90, whereas mouse Dnaaf4 was able to do
305   so (Fig. 3F).
306
307   Given the lack of TPR domain in *Drosophila* Dnaaf4 and its consequent inability to recruit Hsp90,
308   we searched for protein partners that may provide TPR functionality. A GFP-trap affinity purification
309   was carried out on testes expressing the Dnaaf4-mVenus fusion protein. The associated proteins
310   included Pontin (Fig. 4A), which partially corroborates our findings in S2 cells above. However, of
311   the other associated proteins identified, none appeared to have TPR domains or other features that
312   would help clarify Dnaaf4 function. Filtering the data for proteins associated with motile cilia (zur
313   Lage et al., 2021), we found two proteins of interest to be associated but at a P value that is below the
314   threshold for significance (Fig. 4B). Heatr2 (Dnaaf5) is a known dynein assembly factor (Diggle et
315   al., 2014), while *CG13901* is the *Drosophila* orthologue of mouse *Dpcd*, a gene previously linked to
316   ciliary motility and that associates with R2TP (Dafinger et al., 2018). Although these proteins lack
317   TPR domains for direct Hsp90 association, we note that Heatr2/Dnaaf5 has been shown to interact
318   with Dnaaf2 and is proposed to scaffold the formation of a multi-subunit early dynein pre-assembly
319   complex, which could potentially include Hsp90 (Horani et al., 2018).

320   **3.4   *Dnaaf4* and *Dnaaf6* are required for motile ciliated cell function**

321   To determine the functions of *Dnaaf4* and *Dnaaf6*, we initially examined the effects of knockdown
322   using genetically supplied RNA interference. Knockdown of each gene in the male germline (using
323   *BamGal4* driver) resulted in males that produced significantly fewer progeny than controls (Fig. 5A).
324   A climbing assay was used to test the proprioceptive ability and coordination of adult flies.
325   Knockdown of *Dnaaf4* in sensory neurons (UAS-*Dcr2*, *scaGal4*, UAS-*Dnaaf4* RNAi[KK111069])
326   resulted in a significant reduction in climbing ability, consistent with defective chordotonal neuron
327   function (Fig. 6A). Similar reduction was seen for *Dnaaf6* (UAS-*Dcr2*, *scaGal4*, UAS-*Dnaaf6*
328   RNAi[KK108561]) (Fig. 6B).
329
330   To confirm these phenotypes, CRISPR/Cas9 null mutants for *Dnaaf4* and *Dnaaf6* were generated, in
331   which the open reading frame of each gene was replaced with the mini-*white* gene through
332   homology-directed repair. For both *Dnaaf4* and *Dnaaf6,* homozygous null mutant flies are viable
333   with no morphological defects, supporting the hypothesis that they are not required for general
334   cellular functions. However, both *Dnaaf4* and *Dnaaf6* null males are infertile (Fig. 5B–D).
335   Dissection of testes showed normal anatomy but a complete lack of motile sperm (Fig. 5E–I). In
336   *Dnaaf4* null males, the development of motile sperm was rescued by the Dnaaf4-mVenus transgene
337   (Fig. 5C,G). However, the Dnaaf6-mVenus transgene did not rescue the fertility of *Dnaaf6* males
338   (Fig. 5D).
339
340   In a climbing assay, *Dnaaf4* and *Dnaaf6* homozygous null flies showed significant impairment
341   compared to controls, consistent with defective chordotonal neuron function in proprioception (Fig.
342   6C,D). Climbing ability of null flies was restored fully or partially by Dnaaf4-mVenus and Dnaaf6-
343   mVenus transgenes respectively (Fig. 6E,F).
344

345   To assess the auditory function of chordotonal neurons, a larval hearing assay was performed. Third-
346   instar larvae normally respond to a 1000-Hz sine wave tone by momentarily contracting, a behaviour
347   that requires functional dynein motors for mechanotransduction within chordotonal neuron cilia (zur
348   Lage et al., 2021). Larvae homozygous for *Dnaaf4* or *Dnaaf6* mutations did not respond to a tone
349   stimulus, consistent with functionally impaired chordotonal neurons in vibration sensing (Fig. 6G,H).

350   **3.5   Axonemal dyneins are defective in *Dnaaf4* and *Dnaaf6* mutant cilia**

351   Overall, the phenotypes for *Dnaaf4* and *Dnaaf6* null flies are consistent with loss of dynein-driven
352   motility in chordotonal neurons and sperm. To examine this further, TEM was performed on the
353   chordotonal neuron array in the adult antenna (Johnston's Organ) of *Dnaaf4* null mutant flies. This
354   revealed largely normal neuronal structures including well-formed cilia, suggesting that there is no
355   disruption of neuronal differentiation or general ciliogenesis. However, ODA and IDA were strongly
356   reduced or absent (Fig. 7A,B). In antennae from *Dnaaf6* knockdown flies, TEM showed a strong
357   reduction of IDAs and to a lesser extent ODAs (Fig. 7C,D).
358
359   We extended these observations by examining the localisation of dynein markers in chordotonal
360   neurons of pupal antennae. The ODA heavy chain, Dnah5, showed a complete loss of ciliary
361   localisation in both *Dnaaf4* and *Dnaaf6* mutants (Fig. 7E–H). For *Dnaaf4*, similar loss was observed
362   for the ODA light chain marker, Dnal1-mVenus (Fig. 7I,J). A marker of IDA subsets a,c,d, Dnali1-
363   mVenus (light-intermediate chain 1), showed partial loss in ciliary localisation, which was more
364   pronounced in *Dnaaf4* than *Dnaaf6* mutants (Fig. 7K–N). In contrast, the cilium localised TRPV
365   channel subunit, Iav, was not altered in *Dnaaf4* mutants (Fig. 7O,P), suggesting that disruption of
366   ciliary protein localisation is restricted to dynein complexes. Together, these observations suggest
367   that both genes are required specifically for ciliary localisation of axonemal dyneins.
368
369   To investigate further, we assessed changes in protein abundance in *Dnaaf4* knock-down testes by
370   label free quantitative mass spectrometry. In such experiments, a reduction in dynein chains has been
371   considered consistent with instability resulting from defective cytoplasmic pre-assembly (zur Lage et
372   al., 2018; zur Lage et al., 2021). Proteins detected in *Dnaaf4* knock-down testes were compared with
373   control testes, and then filtered to concentrate on those associated with ciliary motility (dynein
374   motors, nexin-dynein regulatory complex, radial spokes, etc (zur Lage et al., 2019)). As expected,
375   Dnaaf4 protein is strongly depleted in knockdown testes ((log2(FC)=-8.69) (Fig. 8A). Of the other
376   ciliary proteins detected, we found a small reduction in several ODA and IDA heavy chains,
377   including kl-3 (orthologue: DNAH8, ODA), Dnah3 (DNAH3, IDA subsets a,b,c,e) and Dhc16F
378   (DNAH6, IDA subset g). Also reduced were CG15128 (paralogue of TTC25, ODA docking
379   complex), CG10750 (CCDC43B, MIA complex) and CG13168 (IQCD, Nexin-DRC). This may
380   reflect a reduction in axonemal stability that appears to be characteristic of dynein loss in
381   spermiogenesis (zur Lage et al., 2021). Interestingly, there is a small increase in Dnaaf2, which is one
382   of the potential partners of Dnaaf4. To compare with the phenotype of another DNAAF, we also
383   determined protein changes upon knockdown of TPR-containing *Spag1* (zur Lage et al., 2018). After
384   filtering for motile ciliary proteins, we found very little difference in protein abundances between
385   *Dnaaf4* and *Spag1* knockdown testes, suggesting that the roles of these DNAAFs are similar, or at
386   least not distinguishable by this technique (Fig. 8B).

387   **4   DISCUSSION**
388
389   *Drosophila Dnaaf4* and *Dnaaf6* are both required for axonemal dynein localisation within cilia,
390   showing that despite the truncated nature of *Dnaaf4*, there is conservation of the roles assigned to

391 homologues in other organisms. Physical evidence supports the possibility that they perform this role
392 together in *Drosophila* as part of an R2TP-like complex that may include Pontin and Reptin (Ruvbl1
393 and 2). On the other hand, for neither gene do we find evidence of function beyond the differentiation
394 of motile cilia, suggesting that in *Drosophila* at least, the role of these genes is specific to axonemal
395 dynein assembly.
396
397 Vertebrate DNAAF4 is predicted to recruit HSP90 via its TPR domain, and we show that mouse
398 Dnaaf4 is able to bind Hsp90. It is remarkable, therefore, that despite apparent conservation of
399 function as an Hsp90 co-chaperone, *Drosophila* Dnaaf4 protein lacks the TPR domain and does not
400 bind Hsp90. Perhaps an accessory TPR-containing protein works with *Drosophila* Dnaaf4.
401 Interestingly, *Drosophila* Spag1 is also strongly truncated, but in this case the truncation retains the
402 TPR domain and not much else (zur Lage et al., 2019). Does Spag1 work in partnership with
403 Dnaaf4? Our proteomic analysis of knockdown testes suggests that Dnaaf4 and Spag1 have similar
404 phenotypes. However, affinity purification analysis did not detect Spag1 as a Dnaaf4-interacting
405 protein. On the other hand, this analysis also did not detect interaction with Dnaaf6, and so the
406 conditions of the assay may not be conducive to identifying Dnaaf4 protein interactors efficiently.
407
408 There are questions regarding the role of the DNAAF4 TPR domain in humans too, since the protein
409 exists in several isoforms with varying numbers of repeats in its TPR domain (Fig. 1B). While
410 isoform-a (which associates with DNAAF2) has a full 3-repeat TPR domain that is likely to be
411 essential for HSP90 binding (Maurizy et al., 2018; Takar et al., 2013), isoform-c (which associates
412 with DNAAF6) has only a single repeat (Maurizy et al., 2018; Paff et al., 2017). It seems unlikely
413 that the limited TPR domain of isoform-c can bind HSP90 directly, and so it may not differ
414 functionally from the *Drosophila* protein so strongly after all.
415
416 Interestingly, *Drosophila* truncated Dnaaf4 resembles the protein that would potentially be
417 synthesised from the human gene bearing the pathogenic mutation detected in PCD: in the original
418 report, 7 out of 9 *DNAAF4* variants in PCD patients were nonsense mutations predicted to encode a
419 truncated protein lacking TPR domains (Tarkar et al., 2013). However, as nonsense-mediated decay
420 (NMD) of the transcript is thought to occur, it is likely that no protein is produced. The finding that
421 *Drosophila* truncated *Dnaaf4* is functional without a TPR domain raises the possibility that inhibition
422 of NMD could restore some function to PCD patients with DNAAF truncating mutations, even if the
423 protein produced lacks the TPR domain. On the other hand, we found in our heterologous expression
424 system that the full TPR domain of mouse Dnaaf4 was required for strong interaction with Dnaaf6.
425
426 We find that *Drosophila* mutants of *Dnaaf4* and *Dnaaf6* show similar loss of dynein markers. While
427 the markers available in *Drosophila* are limited, this finding supports them working in the same
428 complex. There is a strong loss of ODA markers (Dnal1 and Dnah5 homologues) but a partial loss of
429 IDA marker, Dnali1. This chain is predicted to be a subunit of single-headed IDA subsets a, c and d,
430 although it is not certain that d exists in *Drosophila* (zur Lage et al., 2019). In comparison, electron
431 tomography analysis of human PIH1D3-mutant respiratory cilia showed a loss of subset g but no
432 effect on subsets a or c (Olcese et al., 2017). Mutations of the Dnaaf4 homologue in *Chlamydomonas*
433 resulted in strong reduction of most IDA subsets but a weak reduction of subset a (Yamamoto et al.,
434 2017). In other organisms, homologues of these DNAAFs have also been proposed to have a role in
435 the assembly of subset g. For further precision on the subsets affected in *Drosophila*, it would be
436 desirable to generate heavy chain markers for IDA subsets such as antibody raised against the IDA
437 heavy chain DNAH6 homologue, *Dhc16*. Dnaaf4 is proposed to function with Dnaaf2 in addition to
438 Dnaaf6, and it is not known whether this would be responsible for the assembly of other dynein

439 complexes. Given that Dnali1 expression appears lower in the *Dnaaf4* mutant than the *Dnaaf6*
440 mutant, this may also suggest a role for Dnaaf4 partners with proteins in addition to Dnaaf6.
441
442 Several DNAAFs are suspected of having additional non-ciliary functions. For example, mice
443 *DNAAF2* homozygotes are reported to be embryonic lethal (Cheong et al., 2019) consistent with
444 wider roles, and it may be significant that only a small number of PCD patients have been identified
445 with mutations in *DNAAF2* (Omran et al., 2008). In *Drosophila*, *Dnaaf2* (*nop17l*) appears to be
446 widely expressed in embryos (zur Lage et al., 2019), supporting the possibility of widespread roles
447 for this *DNAAF*. In contrast, *Drosophila Dnaaf4* is specifically expressed in motile ciliated cells
448 supporting the hypothesis that has no other roles than facilitating axonemal dynein assembly. In this
449 light it is interesting to consider the roles proposed for vertebrate *DNAAF4*. Truncating mutations of
450 *DNAAF4* were first identified as a candidate causative gene for dyslexia through a role in brain
451 development and maturation (Taipale et al., 2003). Based on rodent models, it has been proposed that
452 *DNAAF4* mutation affects neuronal migration in the developing neocortex (Wang et al., 2006) The
453 link between *DNAAF4* and dyslexia requires further confirmation since this gene did not associate
454 with dyslexia in follow-up studies on other populations (Marino et al., 2005; Scerri, 2004). It is not
455 immediately clear how such a phenotype depends on ciliary motility, raising the possibility that
456 *DNAAF4* may have additional non-ciliary roles. Alternatively, a potential role in neuronal
457 migration/dyslexia could also be an indirect effect of a motile cilia defect, since ciliary motility is
458 required for CSF flow (Kumar et al., 2021). Another intriguing possibility arises from the
459 observation that neuropsychiatric disorders such as schizophrenia, autism and dyslexia have been
460 connected to left-right asymmetry (Trulioff et al., 2017; Valente et al., 2014), which is determined
461 via motile cilia in the embryonic node. Indeed, a recent case report of mutations in the dynein heavy
462 chain genes, *DNAH5* and *DNAH11* has raised the possibility of a link between situs inversus and
463 developmental dyslexia (Bieder et al., 2020).

5   Conflict of Interest

465 The authors declare that the research was conducted in the absence of any commercial or financial
466 relationships that could be construed as a potential conflict of interest.

6   Author Contributions

468 JL conducted many of the experiments and data analysis, contributed to experimental design; PzL
469 conducted S2 cell analysis and contributed to mVenus construction and analysis; AvK provided the
470 mass spectrometry analyses; APJ conducted data analysis, contributed to experimental design, and
471 wrote the manuscript. All authors contributed to manuscript revision, read and approved the
472 submitted manuscript.

available on the preprint server BioRxiv, doi:10.1101/2022.05.12.491607. For the purpose of open access, the authors have applied a Creative Commons Attribution (CC BY) licence to any Author Accepted Manuscript version arising from this submission.

9   Data Availability Statement

The mass spectrometry datasets generated for this study can be found in the ProteomeXchange Consortium via the PRIDE (Perez-Riverol et al., 2019) partner repository with the dataset identifier PXD033608.

10   REFERENCES

Baker, N. E., Yu, S. and Han, D. (1996). Evolution of proneural atonal expression during distinct regulatory phases in the developing Drosophila eye. *Curr. Biol.* **6**, 1290–1302.

Bateman, A., Martin, M.-J., Orchard, S., Magrane, M., Agivetova, R., Ahmad, S., Alpi, E., Bowler-Barnett, E. H., Britto, R., Bursteinas, B., et al. (2021). UniProt: the universal protein knowledgebase in 2021. *Nucleic Acids Res.* **49**, D480–D489.

Bieder, A., Einarsdottir, E., Matsson, H., Nilsson, H. E., Eisfeldt, J., Dragomir, A., Paucar, M., Granberg, T., Li, T.-Q., Lindstrand, A., et al. (2020). Rare variants in dynein heavy chain genes in two individuals with situs inversus and developmental dyslexia: a case report. *BMC Med. Genet.* **21**, 87.

Braschi, B., Omran, H., Witman, G. B., Pazour, G. J., Pfister, K. K., Bruford, E. A. and King, S. M. (2022). Consensus nomenclature for dyneins and associated assembly factors. *J. Cell Biol.* **221**,.

Chagot, M.-E., Dos Santos Morais, R., Dermouche, S., Lefebvre, D., Manival, X., Chipot, C., Dehez, F. and Quinternet, M. (2019). Binding properties of the quaternary assembly protein SPAG1. *Biochem. J.* **476**, 1679–1694.

Cheong, A., Degani, R., Tremblay, K. D. and Mager, J. (2019). A null allele of Dnaaf2 displays embryonic lethality and mimics human ciliary dyskinesia. *Hum. Mol. Genet.* **28**, 2775–2784.

Dafinger, C., Rinschen, M. M., Borgal, L., Ehrenberg, C., Basten, S. G., Franke, M., Höhne, M., Rauh, M., Göbel, H., Bloch, W., et al. (2018). Targeted deletion of the AAA-ATPase Ruvbl1 in mice disrupts ciliary integrity and causes renal disease and hydrocephalus. *Exp. Mol. Med.* **50**, 1–17.

Dietzl, G., Chen, D., Schnorrer, F., Su, K., Barinova, Y., Fellner, M., Gasser, B., Kinsey, K., Oppel, S., Scheiblauer, S., et al. (2007). A genome-wide transgenic RNAi library for conditional gene inactivation in Drosophila. *Nature* **448**, 151–156.

Diggle, C. P., Moore, D. J., Mali, G., zur Lage, P., Ait-Lounis, A., Schmidts, M., Shoemark, A., Garcia Munoz, A., Halachev, M. R., Gautier, P., et al. (2014). HEATR2 Plays a Conserved Role in Assembly of the Ciliary Motile Apparatus. *PLoS Genet.* **10**, e1004577.

Dong, F., Shinohara, K., Botilde, Y., Nabeshima, R., Asai, Y., Fukumoto, A., Hasegawa, T., Matsuo, M., Takeda, H., Shiratori, H., et al. (2014). Pih1d3 is required for cytoplasmic preassembly of axonemal dynein in mouse sperm. *J Cell Biol* **204**, 203–213.

Fabczak, H. and Osinka, A. (2019). Role of the Novel Hsp90 Co-Chaperones in Dynein Arms' Preassembly. *Int. J. Mol. Sci.* **20**, 6174.

Fok, A. K., Wang, H., Katayama, A., Aihara, M. S. and Allen, R. D. (1994). 22S axonemal dynein is preassembled and functional prior to being transported to and attached on the axonemes. *Cell Motil. Cytoskeleton* **29**, 215–224.

Fowkes, M. E. and Mitchell, D. R. (1998). The role of preassembled cytoplasmic complexes in assembly of flagellar dynein subunits. *Mol. Biol. Cell* **9**, 2337–47.

531 **Haslbeck, V., Eckl, J. M., Kaiser, C. J. O., Papsdorf, K., Hessling, M. and Richter, K.** (2013).
532   Chaperone-Interacting TPR Proteins in Caenorhabditis elegans. *J. Mol. Biol.* **425**, 2922–2939.
533 **Horani, A., Ustione, A., Huang, T., Firth, A. L., Pan, J., Gunsten, S. P., Haspel, J. A., Piston, D.**
534   **W. and Brody, S. L.** (2018). Establishment of the early cilia preassembly protein complex
535   during motile ciliogenesis. *Proc. Natl. Acad. Sci.* **115**, E1221–E1228.
536 **Houry, W. A., Bertrand, E. and Coulombe, B.** (2018). The PAQosome, an R2TP-Based
537   Chaperone for Quaternary Structure Formation. *Trends Biochem. Sci.* **43**, 4–9.
538 **Hu, Y., Flockhart, I., Vinayagam, A., Bergwitz, C., Berger, B., Perrimon, N. and Mohr, S. E.**
539   (2011). An integrative approach to ortholog prediction for disease-focused and other functional
540   studies. *BMC Bioinformatics* **12**,.
541 **Kakihara, Y. and Houry, W. A.** (2012). The R2TP complex: discovery and functions. *Biochim.*
542   *Biophys. Acta* **1823**, 101–7.
543 **King, S. M.** (2016). Axonemal Dynein Arms. *Cold Spring Harb. Perspect. Biol.* **8**, a028100.
544 **Krause, S. A., Overend, G., Dow, J. A. T. and Leader, D. P.** (2022). FlyAtlas 2 in 2022:
545   enhancements to the Drosophila melanogaster expression atlas. *Nucleic Acids Res.* **50**, D1010–
546   D1015.
547 **Kumar, S., Stecher, G. and Tamura, K.** (2016). MEGA7: Molecular Evolutionary Genetics
548   Analysis Version 7.0 for Bigger Datasets. *Mol. Biol. Evol.* **33**, 1870–1874.
549 **Kumar, V., Umair, Z., Kumar, S., Goutam, R. S., Park, S. and Kim, J.** (2021). The regulatory
550   roles of motile cilia in CSF circulation and hydrocephalus. *Fluids Barriers CNS* **18**, 31.
551 **Larkin, A., Marygold, S. J., Antonazzo, G., Attrill, H., dos Santos, G., Garapati, P. V,**
552   **Goodman, J. L., Gramates, L. S., Millburn, G., Strelets, V. B., et al.** (2021). FlyBase:
553   updates to the Drosophila melanogaster knowledge base. *Nucleic Acids Res.* **49**, D899–D907.
554 **Li, Y., Zhao, L., Yuan, S., Zhang, J. and Sun, Z.** (2017). Axonemal dynein assembly requires the
555   R2TP complex component Pontin. *Development* dev.152314.
556 **Liu, G., Wang, L. and Pan, J.** (2019). Chlamydomonas WDR92 in association with R2TP-like
557   complex and multiple DNAAFs to regulate ciliary dynein preassembly. *J. Mol. Cell Biol.* **11**,
558   770–780.
559 **Marino, C., Giorda, R., Luisa Lorusso, M., Vanzin, L., Salandi, N., Nobile, M., Citterio, A.,**
560   **Beri, S., Crespi, V., Battaglia, M., et al.** (2005). A family-based association study does not
561   support DYX1C1 on 15q21.3 as a candidate gene in developmental dyslexia. *Eur. J. Hum.*
562   *Genet.* **13**, 491–499.
563 **Martino, F., Pal, M., Muñoz-Hernández, H., Rodríguez, C. F., Núñez-Ramírez, R., Gil-Carton,**
564   **D., Degliesposti, G., Skehel, J. M., Roe, S. M., Prodromou, C., et al.** (2018). RPAP3 provides
565   a flexible scaffold for coupling HSP90 to the human R2TP co-chaperone complex. *Nat.*
566   *Commun.* **9**, 1501.
567 **Maurizy, C., Quinternet, M., Abel, Y., Verheggen, C., Santo, P. E., Bourguet, M., Paiva, A. C.**
568   **F., Bragantini, B., Chagot, M. E., Robert, M. C., et al.** (2018). The RPAP3-Cterminal domain
569   identifies R2TP-like quaternary chaperones. *Nat. Commun.* **9**,.
570 **Moore, D. J., Onoufriadis, A., Shoemark, A., Simpson, M. A., Zur Lage, P. I., De Castro, S. C.,**
571   **Bartoloni, L., Gallone, G., Petridi, S., Woollard, W. J., et al.** (2013). Mutations in
572   ZMYND10, a gene essential for proper axonemal assembly of inner and outer dynein arms in
573   humans and flies, cause primary ciliary dyskinesia. *Am. J. Hum. Genet.* **93**, 346–356.
574 **Newton, F. G., zur Lage, P. I., Karak, S., Moore, D. J., Göpfert, M. C. and Jarman, A. P.**
575   (2012). Forkhead Transcription Factor Fd3F Cooperates with Rfx to Regulate a Gene
576   Expression Program for Mechanosensory Cilia Specialization. *Dev. Cell* **22**, 1221–1233.
577 **Olcese, C., Patel, M. P., Shoemark, A., Kiviluoto, S., Legendre, M., Williams, H. J., Vaughan,**
578   **C. K., Hayward, J., Goldenberg, A., Emes, R. D., et al.** (2017). X-linked primary ciliary
579   dyskinesia due to mutations in the cytoplasmic axonemal dynein assembly factor PIH1D3. *Nat.*

580   *Commun.* **8**,.

581   **Omran, H., Kobayashi, D., Olbrich, H., Tsukahara, T., Loges, N. T., Hagiwara, H., Zhang, Q.,**
582   **Leblond, G., O'Toole, E., Hara, C., et al.** (2008). Ktu/PF13 is required for cytoplasmic pre-
583   assembly of axonemal dyneins. *Nature* **456**, 611–6.

584   **Paff, T., Loges, N. T., Aprea, I., Wu, K., Bakey, Z., Haarman, E. G., Daniels, J. M. A.,**
585   **Sistermans, E. A., Bogunovic, N., Dougherty, G. W., et al.** (2017). Mutations in PIH1D3
586   Cause X-Linked Primary Ciliary Dyskinesia with Outer and Inner Dynein Arm Defects. *Am. J.*
587   *Hum. Genet.* **100**, 160–168.

588   **Pal, M., Morgan, M., Phelps, S. E. L., Roe, S. M., Parry-Morris, S., Downs, J. A., Polier, S.,**
589   **Pearl, L. H. and Prodromou, C.** (2014). Structural basis for phosphorylation-dependent
590   recruitment of Tel2 to Hsp90 by Pih1. *Structure* **22**, 805–18.

591   **Perez-Riverol, Y., Csordas, A., Bai, J., Bernal-Llinares, M., Hewapathirana, S., Kundu, D. J.,**
592   **Inuganti, A., Griss, J., Mayer, G., Eisenacher, M., et al.** (2019). The PRIDE database and
593   related tools and resources in 2019: Improving support for quantification data. *Nucleic Acids*
594   *Res.* **47**, D442–D450.

595   **Scerri, T. S.** (2004). Putative functional alleles of DYX1C1 are not associated with dyslexia
596   susceptibility in a large sample of sibling pairs from the UK. *J. Med. Genet.* **41**, 853–857.

597   **Sitaram, P., Hainline, S. G. and Lee, L. A.** (2014). Cytological Analysis of Spermatogenesis: Live
598   and Fixed Preparations of Drosophila Testes. *J. Vis. Exp.* **83**,.

599   **Smith, A. J., Bustamante-Marin, X. M., Yin, W., Sears, P. R., Herring, L. E., Dicheva, N. N.,**
600   **López-Giráldez, F., Mane, S., Tarran, R., Leigh, M. W., et al.** (2022). The role of SPAG1 in
601   the assembly of axonemal dyneins in human airway epithelia. *J. Cell Sci.* **135**,.

602   **Taipale, M., Kaminen, N., Nopola-Hemmi, J., Haltia, T., Myllyluoma, B., Lyytinen, H., Muller,**
603   **K., Kaaranen, M., Lindsberg, P. J., Hannula-Jouppi, K., et al.** (2003). A candidate gene for
604   developmental dyslexia encodes a nuclear tetratricopeptide repeat domain protein dynamically
605   regulated in brain. *Proc. Natl. Acad. Sci.* **100**, 11553–11558.

606   **Tarkar, A., Loges, N. T., Slagle, C. E., Francis, R., Dougherty, G. W., Tamayo, J. V, Shook, B.,**
607   **Cantino, M., Schwartz, D., Jahnke, C., et al.** (2013). DYX1C1 is required for axonemal
608   dynein assembly and ciliary motility. *Nat. Genet.* **45**, 995–1003.

609   **Trulioff, A., Ermakov, A. and Malashichev, Y.** (2017). Primary Cilia as a Possible Link between
610   Left-Right Asymmetry and Neurodevelopmental Diseases. *Genes (Basel).* **8**, 48.

611   **Valente, E. M., Rosti, R. O., Gibbs, E. and Gleeson, J. G.** (2014). Primary cilia in
612   neurodevelopmental disorders. *Nat. Rev. Neurol.* **10**, 27–36.

613   **Vaughan, C. K.** (2014). Hsp90 Picks PIKKs via R2TP and Tel2. *Structure* **22**, 799–800.

614   **Vieillard, J., Paschaki, M., Duteyrat, J. L., Augière, C., Cortier, E., Lapart, J. A., Thomas, J.**
615   **and Durand, B.** (2016). Transition zone assembly and its contribution to axoneme formation in
616   Drosophila male germ cells. *J. Cell Biol.* **214**, 875–889.

617   **Wang, Y., Paramasivam, M., Thomas, A., Bai, J., Kaminen-Ahola, N., Kere, J., Voskuil, J.,**
618   **Rosen, G. D., Galaburda, A. M. and Loturco, J. J.** (2006). DYX1C1 functions in neuronal
619   migration in developing neocortex. *Neuroscience* **143**, 515–522.

620   **Xiang, W., zur Lage, P., Newton, F. G., Qiu, G. and Jarman, A. P.** (2022). The dynamics of
621   protein localisation to restricted zones within Drosophila
622   mechanosensory cilia. *bioRxiv* 2022.03.02.482694.

623   **Yamaguchi, H., Oda, T., Kikkawa, M. and Takeda, H.** (2018). Systematic studies of all PIH
624   proteins in zebrafish reveal their distinct roles in axonemal dynein assembly. *Elife* **7**,.

625   **Yamamoto, R., Hirono, M. and Kamiya, R.** (2010). Discrete PIH proteins function in the
626   cytoplasmic preassembly of different subsets of axonemal dyneins. *J. Cell Biol.* **190**, 65–71.

627   **Yamamoto, R., Obbineni, J. M., Alford, L. M., Ide, T., Owa, M., Hwang, J., Kon, T., Inaba, K.,**
628   **James, N., King, S. M., et al.** (2017). Chlamydomonas DYX1C1/PF23 is essential for

629   axonemal assembly and proper morphology of inner dynein arms. *PLoS Genet.* **13**, 1–21.

630 **Yamamoto, R., Yanagi, S., Nagao, M., Yamasaki, Y., Tanaka, Y., Sale, W. S., Yagi, T. and Kon,**

631   **T.** (2020). Mutations in PIH proteins MOT48, TWI1 and PF13 define common and unique steps

632   for preassembly of each, different ciliary dynein. *PLOS Genet.* **16**, e1009126.

633 **Zhao, R., Davey, M., Hsu, Y. C., Kaplanek, P., Tong, A., Parsons, A. B., Krogan, N., Cagney,**

634   **G., Mai, D., Greenblatt, J., et al.** (2005). Navigating the chaperone network: An integrative

635   map of physical and genetic interactions mediated by the hsp90 chaperone. *Cell* **120**, 715–727.

636 **Zhao, L., Yuan, S., Cao, Y., Kallakuri, S., Li, Y., Kishimoto, N., DiBella, L. and Sun, Z.** (2013).

637   Reptin/Ruvbl2 is a Lrrc6/Seahorse interactor essential for cilia motility. *Proc. Natl. Acad. Sci.*

638   **110**, 12697–12702.

639 **zur Lage, P., Stefanopoulou, P., Styczynska-Soczka, K., Quinn, N., Mali, G., von Kriegsheim,**

640   **A., Mill, P. and Jarman, A. P.** (2018). Ciliary dynein motor preassembly is regulated by

641   Wdr92 in association with HSP90 co-chaperone, R2TP. *J. Cell Biol.* **217**, 2583–2598.

642 **zur Lage, P., Newton, F. G. and Jarman, A. P.** (2019). Survey of the Ciliary Motility Machinery of

643   Drosophila Sperm and Ciliated Mechanosensory Neurons Reveals Unexpected Cell-Type

644   Specific Variations: A Model for Motile Ciliopathies. *Front. Genet.* **10**,

645   10.3389/fgene.2019.00024.

646 **zur Lage, P., Xi, Z., Lennon, J., Hunter, I., Chan, W. K., Bolado Carrancio, A., von**

647   **Kriegsheim, A. and Jarman, A. P.** (2021). The Drosophila orthologue of the primary ciliary

648   dyskinesia-associated gene, DNAAF3, is required for axonemal dynein assembly. *Biol. Open*

649   **10**, 10.1242/bio.058812.

650

651

652
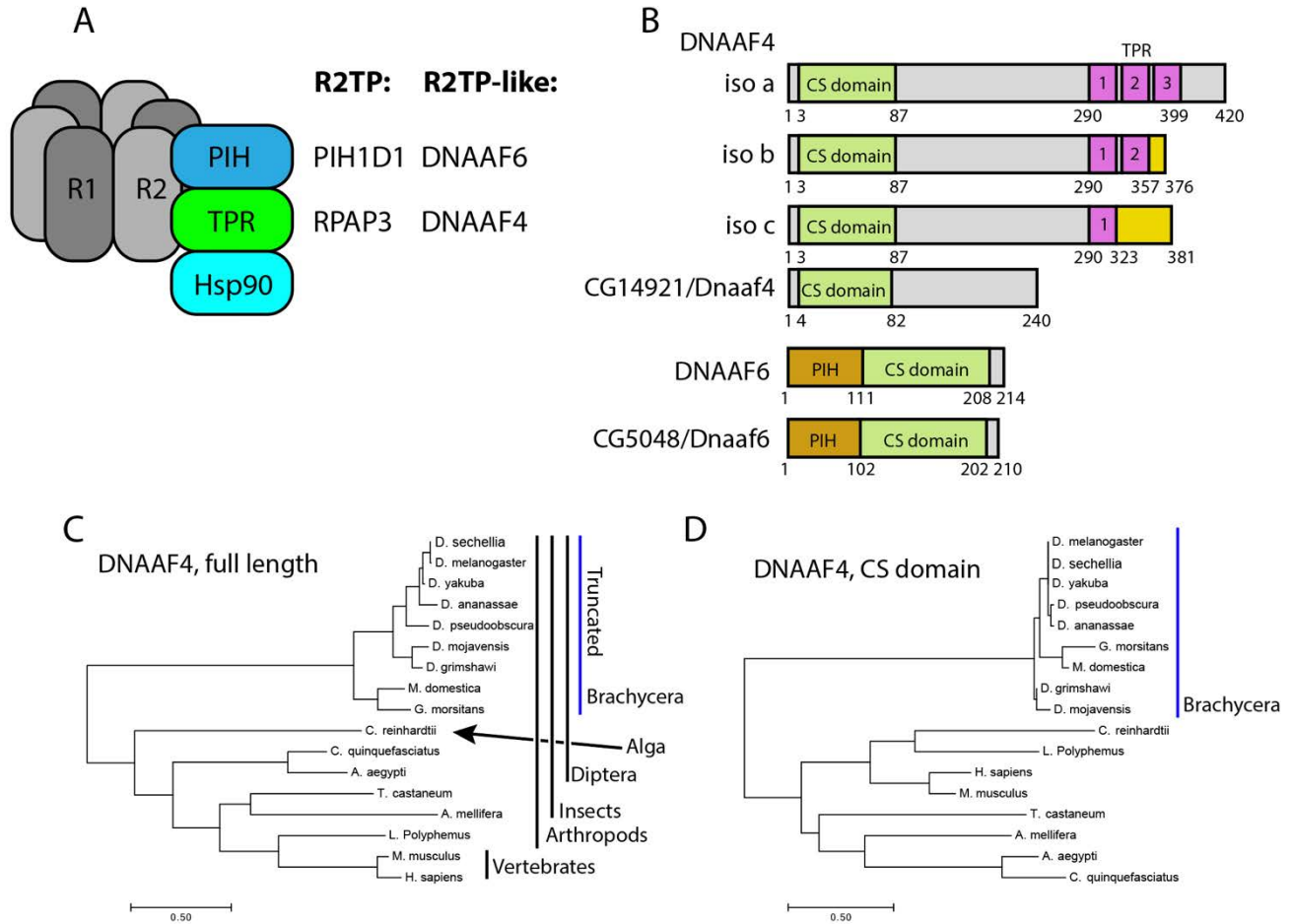
653
654
655 **Figure 1 *Drosophila* and mammalian Dnaaf4/Dnaaf6 proteins.**
656 (A) Schematic showing the composition of R2TP and putative DNAAF4/6-containing R2TP-like
657 complexes. Note that association of DNAAF4/6 with RUVBL1 and RUVBL2 is speculative. (B)
658 Schematic showing the protein domains of human DNAAF4, DNAAF6 and their *Drosophila*
659 orthologues. Human isoforms and protein structures are based on Maurizy et al. (2018). (C)
660 Phylogenetic tree of DNAAF4 sequences from selected species including vertebrates, arthropods and
661 the unicellular green alga, *Chlamydomonas reinhardtii* (established ciliary motility model organism).
662 Higher dipterans (Brachycera) form a distinct group that correlates with gene truncation (blue bar).
663 (D) When comparing CS domains alone, the tree structure remains similar, with Brachycera distinct
664 from other taxa. Organisms included in this tree: *Drosophila sechellia, D. melanogaster, D. yakuba,*
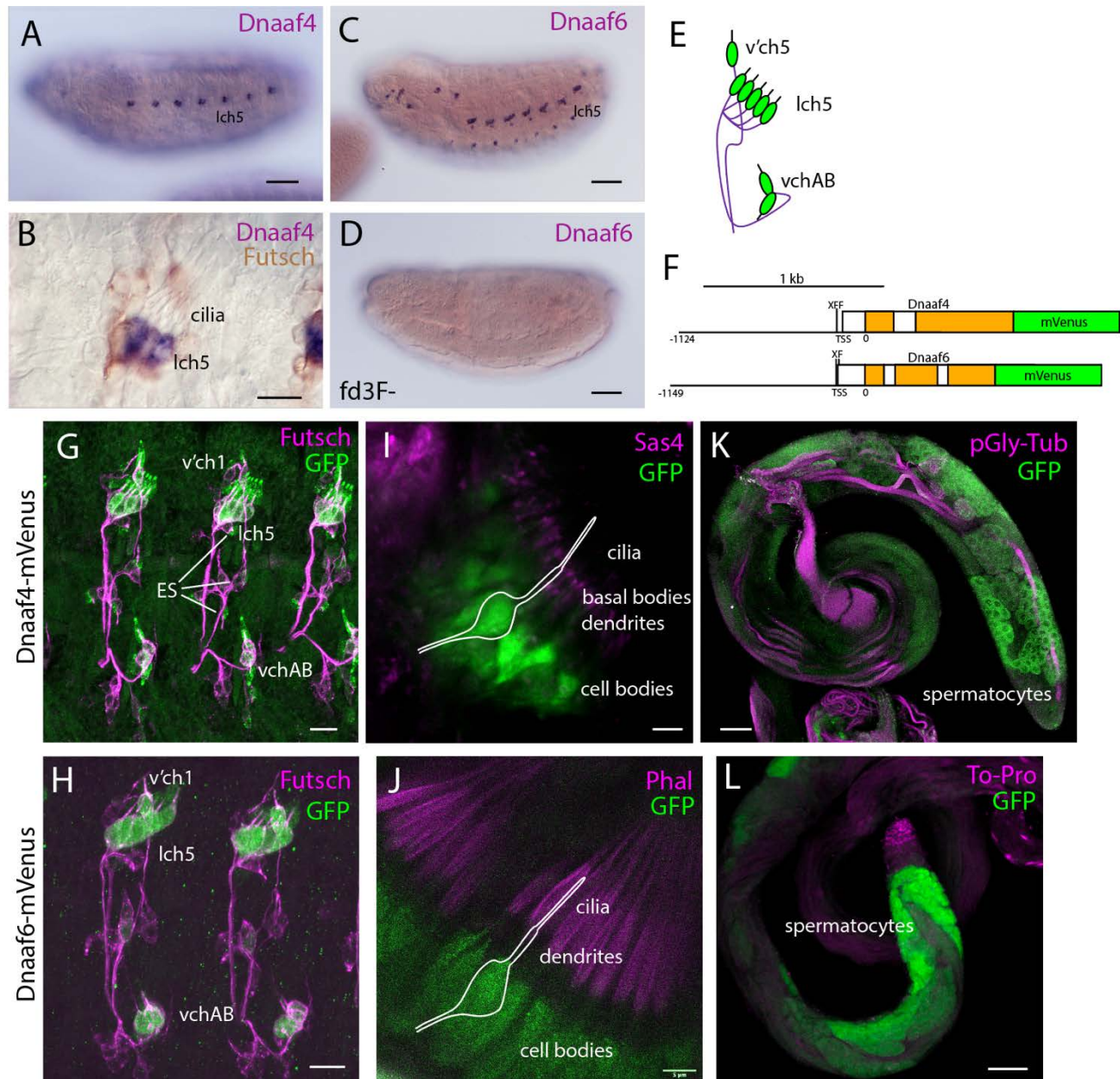665 *D. ananassae, D. pseudoobscura, D. mojavensis, D. grimshawi, Musca domestica, Glossina*
666 *morsitans, Culex quinquefasciatus, Aedes aegypti, Tribolium castaneum, Apis mellifera,*
667 *Chlamydomonas reinhardtii, Limulus polyphemus, Mus musculus* and *Homo sapiens.*
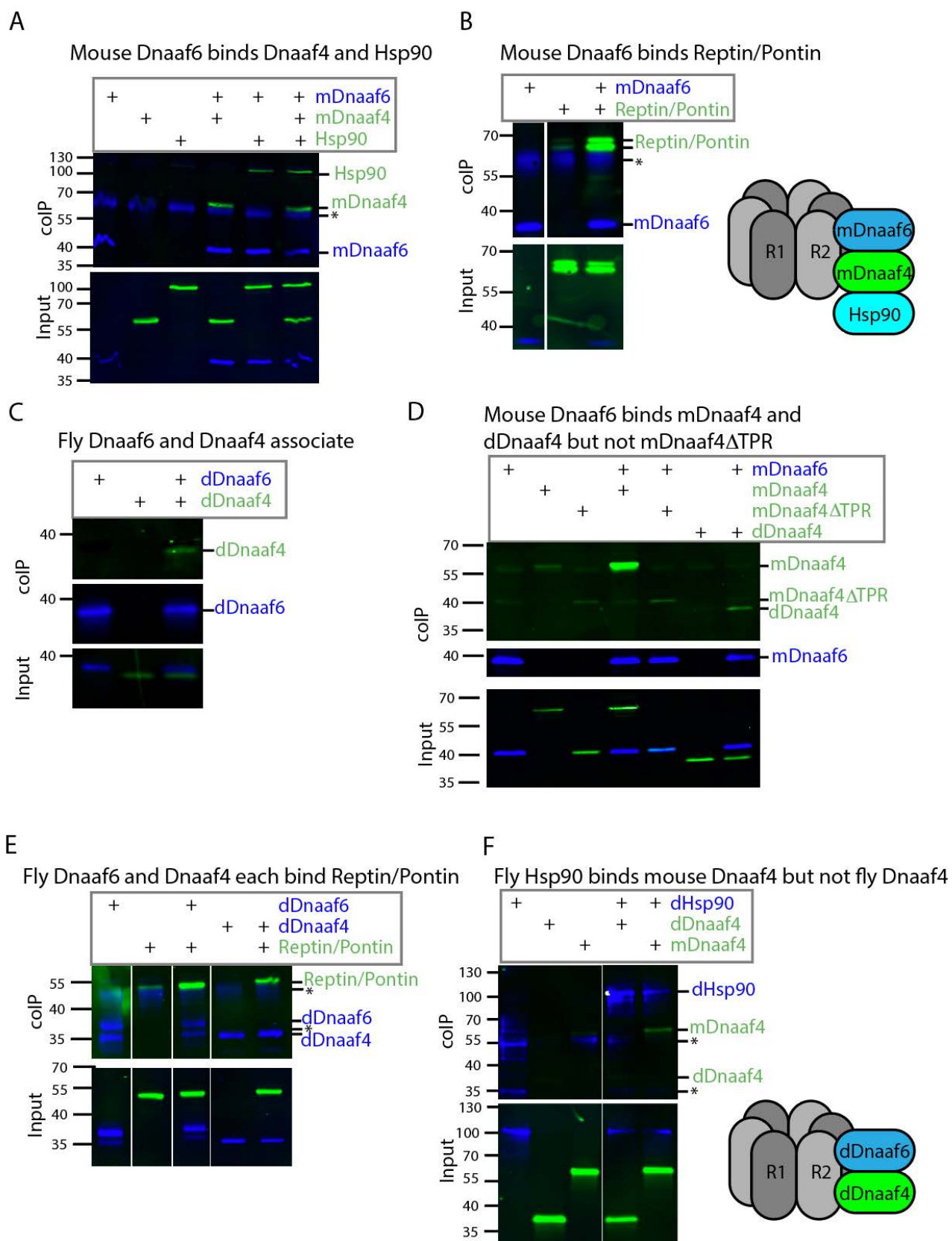668

669

670
671 **Figure 2. Dnaaf4 and Dnaaf6 are both expressed in *Drosophila* motile cilia cells.**
672 (A–D) RNA *in situ* hybridisation (dark blue) conducted on late-stage whole-mount embryos. (A)
673 *Dnaaf4* probe, *Dnaaf4* is expressed specifically in the chordotonal neurons. (B) Higher magnification
674 indicates that this expression becomes restricted at a late stage to a subset of chordotonal neurons
675 (lch5). Here the embryo has been counterstained with antibodies against Futsch (brown), which
676 labels all sensory neurons. (C) *Dnaaf6* shows expression in developing chordotonal neurons. (D) In
677 an embryo homozygous mutant for *fd3F*, expression of *Dnaaf6* is abolished. (E) Schematic of the
678 arrangement of chordotonal neurons in embryonic abdominal segments. (F) Schematic illustrating
679 mVenus fusion transgenes. Each includes 5' flanking DNA containing potential binding sites for the
680 transcription factors fd3f (F) and Rfx (X) (Dnaaf4: CTGTTCACTTG, GTTCACTTGCAGC;
681 Dnaaf6: ACTAAATAAACAA, GTTGCCAGGAAA). (G–L) Expression of Dnaaf4-mVenus
682 detected by anti-GFP antibodies. (G,H) Late embryos counterstained with anti-Futsch (magenta)
683 show expression of both fusion genes in chordotonal neurons. In the case of Dnaaf4-mVenus, some

684   expression is observed in some external sensory (ES) neurons. As this is not observed for the mRNA,
685   it is likely an artefact of the expression construct. (I,J) In pupal antennae, both fusion genes are
686   expressed in the cell bodies of chordotonal neurons that form Johnston's Organ. A schematic of
687   approximate neuronal location is shown. The counterstain (magenta) is the basal body marker Sas4
688   (I) or phalloidin (J), which marks the actin basket (scolopale) that surrounds the cilia. (K,L) In adult
689   testes, both fusion genes are expressed in differentiating germline cells (spermatocytes and
690   spermatids). Counterstains (magenta) are polyglycylated tubulin (K) or To-Pro (L). Scale bars are:
691   (A,C,D,K,L) 50 μm (B,G,H) 10 μm (I,J) 5 μm. Number of samples imaged: (G) $n = 7$ (I) $n = 9$ (K) n
692     $= 8$.

A Mouse Dnaaf6 binds Dnaaf4 and Hsp90

B Mouse Dnaaf6 binds Reptin/Pontin

C Fly Dnaaf6 and Dnaaf4 associate

D Mouse Dnaaf6 binds mDnaaf4 and dDnaaf4 but not mDnaaf4ΔTPR

E Fly Dnaaf6 and Dnaaf4 each bind Reptin/Pontin

F Fly Hsp90 binds mouse Dnaaf4 but not fly Dnaaf4

693

694 **Figure 3. *Drosophila* and mouse Dnaaf4/Dnaaf6 complexes**
695 Coimmunoprecipitations of tagged proteins expressed in S2 cells. In each case, the bait protein is
696 FLAG-tagged (blue) and the prey protein is HA-tagged (green). Proteins are from *Drosophila* unless
697 indicated. 'Input' represents Western blot of whole cell extracts with bait/prey simultaneously
698 detected (anti-FLAG + anti-HA). 'coIP' represents FLAG-mediated coIP followed by simultaneous
699 detection of FLAG- and HA-tagged proteins on Western blot. *indicates non-specific bands. (A)
700 Mouse FLAG-Dnaaf6 protein associates with mouse HA-Dnaaf4 and *Drosophila* HA-Hsp90. (B)
701 Mouse FLAG-Dnaaf6 protein binds *Drosophila* HA-Reptin/HA-Pontin. (C) *Drosophila* FLAG-
702 Dnaaf6 and HA-Dnaaf4 associate. (D) Mouse FLAG-Dnaaf6 binds both mouse HA-Dnaaf4 and
703 *Drosophila* HA-Dnaaf4, but is unable to bind the mouse Dnaaf4 protein with TPR domain deleted
704 (HA-Dnaaf4ΔTPR). (E) *Drosophila* FLAG-Dnaaf6 and FLAG-Dnaaf4 are each capable of binding
705 HA-Reptin/HA-Pontin. (F) Drosophila FLAG-Hsp90 is able to bind mouse HA-Dnaaf4 but not
706 Drosophila HA-Dnaaf4.
707
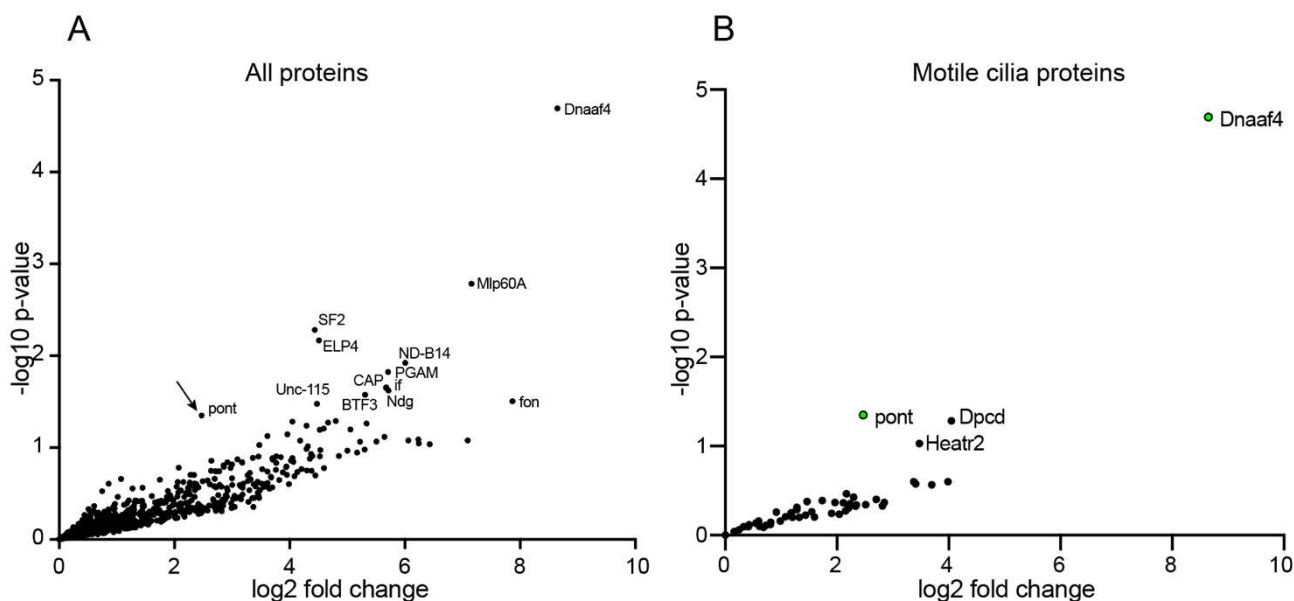
708
709 **Figure 4. Proteins preferentially associated with Dnaaf4 in *Drosophila* testes**
710 Volcano plots of proteins detected by MS after affinity purification of Dnaaf4-mVenus, shown as
711 relative abundance (fold change) compared with proteins associated with unrelated control protein
712 (GAP43-mVenus). (A) All proteins, with those above threshold significance (-log10(p-value)>1.3)
713 labelled. Pontin of R2TP is significantly associated (arrow). (B) The same dataset filtered to extract
714 proteins associated with motile cilia (zur Lage et al., 2021). Pontin is the only associated protein to
715 reach statistical significance. However, two other proteins of interest are just below significance
716 threshold: Dpcd and Heatr2 (Dnaaf5). Significance was determined using the Empirical Bayes
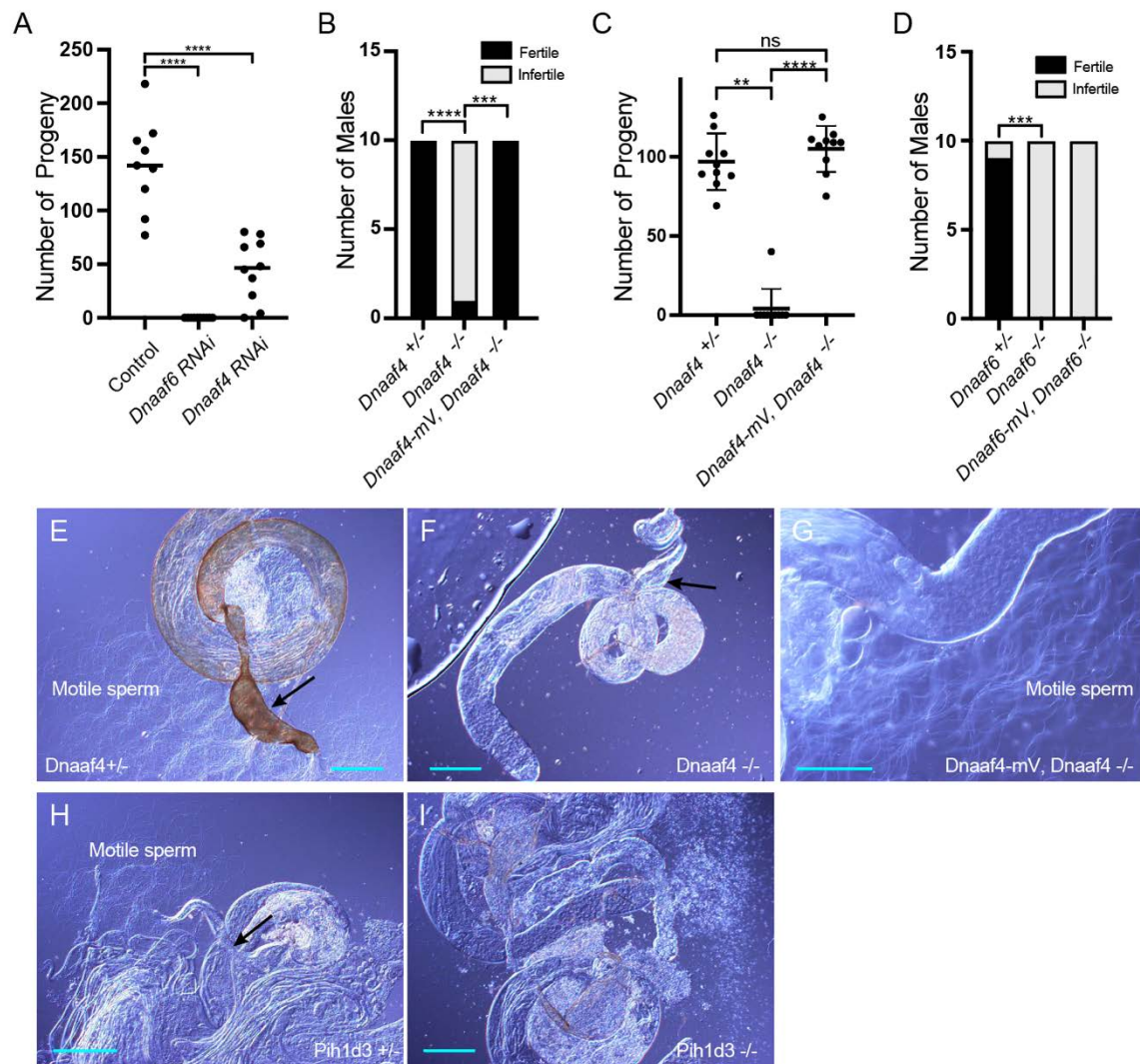717 method. *n* = 150 pairs of testes per replicate; 3 replicates per genotype.
718

Figure 5. Knockdown and Null mutants of *Dnaaf4* and *Dnaaf6* are male infertile.
(A) *Dnaaf4* and *Dnaaf6* RNAi knockdown males (*BamGal4*) produce fewer progeny than control males. Progeny from individual males and median progeny value are shown. Knockdown of either gene significantly reduces progeny per male (P<0.0001, One-way ANOVA followed by Sidak's Test for multiple comparisons). (B,C) Fertility of *Dnaaf4* null mutant males. (B) Proportion of males that are fully infertile. Most *Dnaaf4* mutant males are infertile but this is rescued by the Dnaaf4-mVenus transgene (P=0.001, Fisher's exact test) (C) Number of progeny per male, showing that rescued homozygous males are fully fertile compared with heterozygotes (P>0.9999, Kruskal-Wallis analysis followed by Dunn's test for multiple comparisons). *n* = 10 males for each genotype. (C) Data for males in (B) plotted as number of progeny per male. A single Dnaaf4 homozygote gave progeny, perhaps due to being non-virgin at collection – 40 progeny compared with a mean of 96.9 for heterozygotes. (D) Fertility assay results showing a decrease in the number of fertile males in the *Dnaaf6* null mutant when compared to control groups (0.0001). *Dnaaf6* rescue did not produce progeny (P<0.0001) like that of the homozygous null mutants. *n* = 10 males per genotype. (E–I) Testes and associated male reproductive structures dissected from adult males and observed by light microscopy. Scale bars, 50 μm. (E) *Dnaaf4* heterozygote testis showing S-shaped motile sperm emerging from large (sperm-filled) seminal vesicle (black arrow). (F) *Dnaaf4* homozygote testis showing small (empty) seminal vesicle (black arrow) and absence of motile sperm. (G) Testis from *Dnaaf4* homozygote with *Dnaaf4*-mVenus transgene showing rescue of motile sperm production. (H)

739   *Dnaaf6* heterozygote showing S-shaped motile sperm emerging from large (sperm-filled) seminal
740   vesicle (black arrow). (I) *Dnaaf6* homozygote testes homozygote testis showing absence of motile
741   sperm.
742
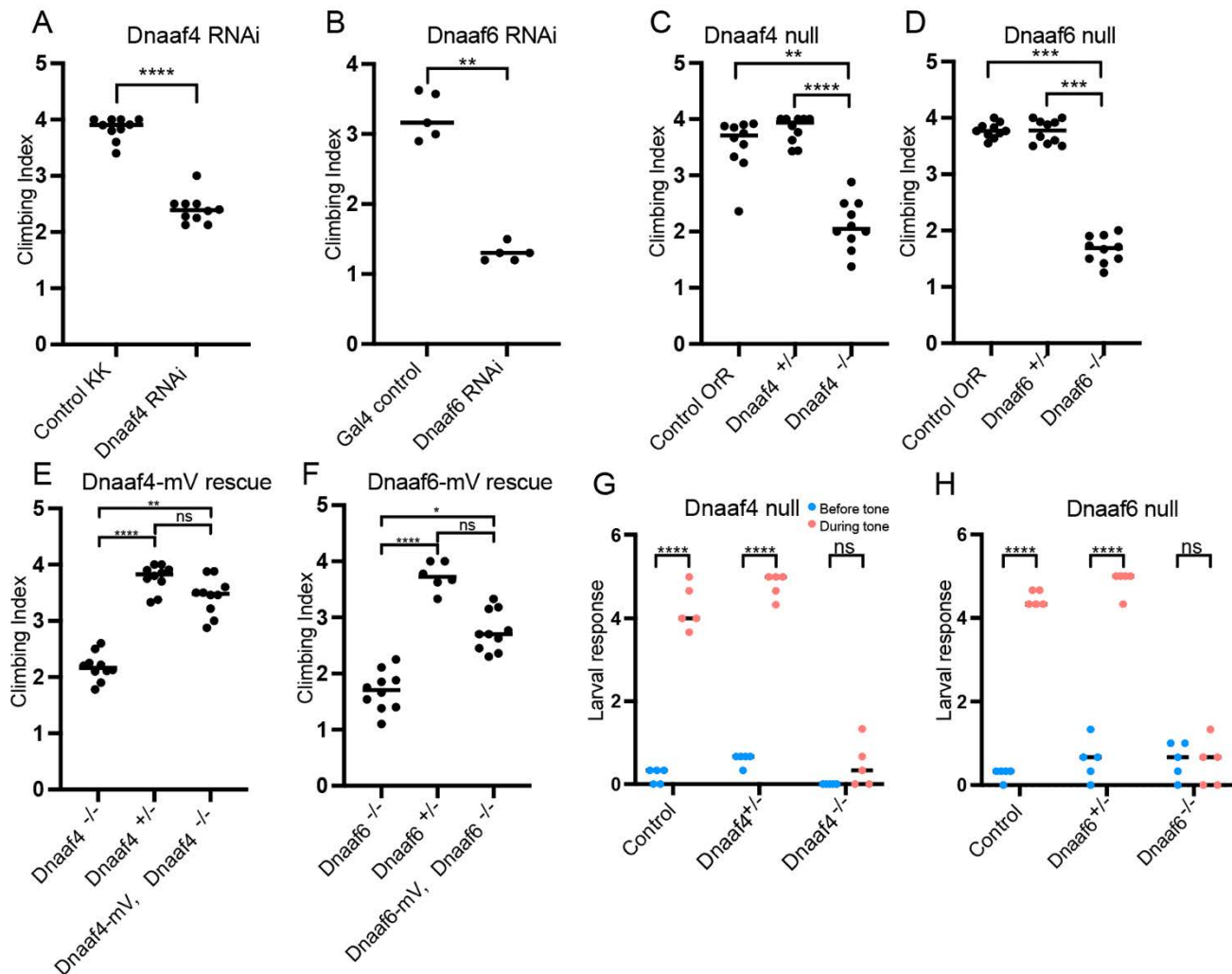
Figure 6. Knockdown and Null mutants of *Dnaaf4* and *Dnaaf6* have defective chordotonal sensory function.
(A–F) Adult climbing assays for proprioceptive ability. Plots (with median and individual values), each point is a batch of 8-12 females, n=10 batches. (A,B) RNAi knockdown of *Dnaaf4* and *Dnaaf6* in sensory neurons (*scaGal4*) results in significant decrease in climbing ability. (C,D) Homozygote null adults for *Dnaaf4* and *Dnaaf6* have significantly decreased climbing ability compared with heterozygotes. (E,F) Rescue of null mutants. (E) *Dnaaf4*-mVenus transgene rescued the climbing ability of *Dnaaf4* null mutant flies, showing a significant increase in climbing performance when compared to null (P= 0.0012), restoring climbing ability to the same level as the heterozygotes (P=0.8130). (F) *Dnaaf6*-mVenus transgene partial restores climbing ability of *Dnaaf6* null mutants (P=0.0103), but not to levels seen in the heterozygote, although the latter difference does not reach significance (P=0.1282). (G,H) Plots (with individual and median values) showing hearing assay performances for *Dnaaf4*^{-/-} and *Dnaaf6*^{-/-} larvae in comparison to heterozygote and wild-type (OrR) controls. Number of larvae contracting before and during a 1000-Hz tone was measured. Individual points are batches of 5 larvae, n=5 batches. There is a significant difference between the number of larvae contracting before and during the tone (P < 0.0001) for control groups of both genotypes. There is no significant difference between the number of contractions occurring before and during the tone for *Dnaaf4* or *Dnaaf6* null mutants, indicating no behavioural response to stimulus. For climbing assays, significance was determined by Kruskal-Wallis followed by Dunn's test for multiple comparisons. For hearing assay, significance was determined by two-way RM ANOVA and

764   Sidak's multiple comparisons test. Statistical significance on plots is indicated by asterisks: *,
765     $P \leq 0.05$; **, $P \leq 0.01$; ***, $P \leq 0.001$; ****, $P \leq 0.0001$.
766
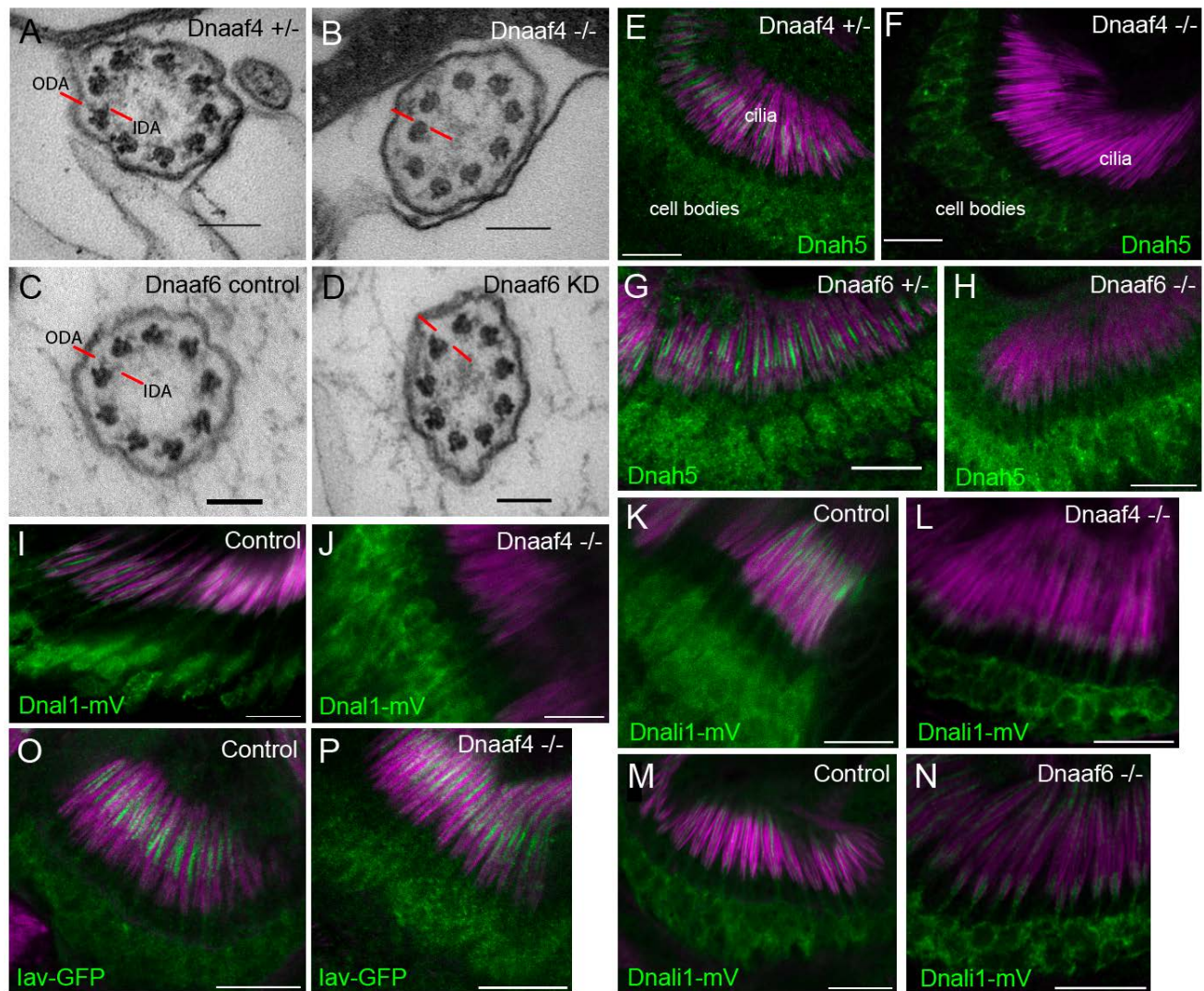
Figure 7. Defective dynein motor localisation in mutants.
(A–D) TEM of chordotonal neurons in adult antennae, transverse sections of cilia showing 9+0 axonemal arrangement. (A) Control (*Dnaaf4*$^{+/-}$ heterozygote) with ODAs and IDAs (red lines) on each microtubule doublet. (B) *Dnaaf4*$^{-/-}$ homozygote showing severe loss of ODA and IDA structures from the microtubule doublets. (C) RNAi control (*scaGal4*, UAS-*Dcr2*, KK line) and (D) *Dnaaf6* knockdown (*scaGal4*, UAS-*Dcr2*, UAS-*Dnaaf6*RNAi). The latter shows a reduction of ODA and IDA. (E-P) Immunofluorescence of ODA/IDA markers (green) in differentiating chordotonal neurons of pupal antennae. All are counterstained with phalloidin, detecting the scolopale structures surrounding the cilia (magenta). (E–H) ODA heavy chain Dnah5 localisation in cilia is lost from *Dnaaf4*$^{-/-}$ and *Dnaaf6*$^{-/-}$ homozygote mutants (F,H) compared to controls (E,G), despite presence of protein in the cell bodies. (I,J) ODA marker, Dnal1-mVenus shows a similar loss of ciliary localisation in *Dnaaf4*$^{-/-}$ homozygote (J) relative to *w*$^-$ control (I). (K–N) IDA marker, Dnali1-mVenus shows a partial loss of ciliary localisation in *Dnaaf4*$^{-/-}$ and *Dnaaf6*$^{-/-}$ homozygotes (L,N) relative to heterozygote controls (K,M). (O,P) TRPV channel subunit Iav shows no difference in ciliary localisation between *Dnaaf4*$^{-/-}$ homozygote (P) and *w*$^-$ control (O). Scale bars: (A–D) 100 nm, (E–P) 10 mm. Number of antennae imaged for IF: (E) n=7; (F) 7; (G) 6; (H) 5; (I) 5; (J) 10; (K) 5; (L) 9; (M) 8; (N) 9; (O) 6; (P) 7.

A

Depleted in *Dnaaf4* KD

TTC25 - CG15128
DNAI1 - CG9313
DNAH3 - Dnah3
DNAH6 - Dhc16F
DNAH7 - Dhc36C
DNAH8 - kl-3
DNAH10 - Dhc98D
WDR78 - Dic61B
WDR63 - CG14838
CCDC43B - CG10750
IQCD - CG13168
DYNLRB1/2 - CG16837
ARMC4 - gudu
CCDC63 - wampa
GAS8 - Gas8
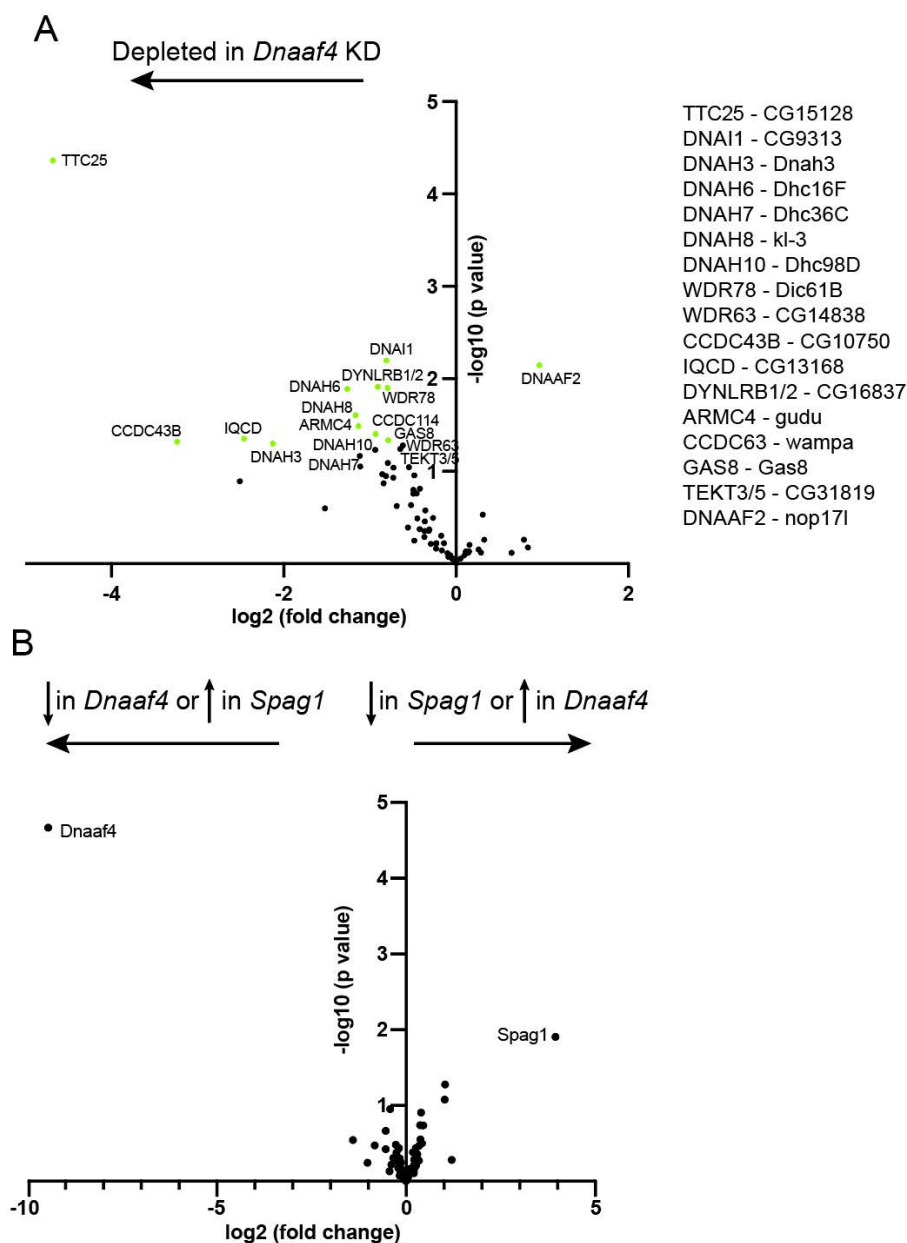TEKT3/5 - CG31819
DNAAF2 - nop17l

B

Figure 8. Proteomic changes in *Dnaaf4* mutant testes

(A) Volcano plot of motile cilia-associated proteins detected by MS in testes. To the left of the Y axis
are proteins that are more less abundant in *Dnaaf4RNAi* KD (*BamGal4,* UAS-*Dnaaf4RNAi*) testes
compared with *BamGal4* control (depleted); to the right are proteins that are more abundant than in
the control. Dnaaf4 protein itself is strongly depleted as expected (log2(FC)=-8.69, -log10(p value)=
4.39) but for clarity it is not shown on plot. Proteins with -log10(p value)>1.3 (green points) are
labelled with names of human homologues. The *Drosophila* gene names are shown to the right. *n* =
30 pairs of testes/replicate; 4 replicates per genotype. (B) Volcano plot comparing motile cilia-
associated proteins detected in testes from *Dnaaf4* knockdown testes compared with *Spag1*
knockdown testes (*BamGal4,* UAS-*Spag1RNAi*). The only proteins showing significant difference in
abundance are Dnaaf4 and Spag1 themselves. Significance was determined using the Empirical
Bayes method. *n* = 30 pairs of testes/replicate; 4 replicates per genotype.

```
801      Fly     2 VQIS-----QTEEDIKISIELNRLVTRKPDVVLLPQYLKFNNPPIFFERHLAQEIDEMASFCRIF 61
802                :|:|        ||:..:.:|:.|..:.,|..||....,|||.|.||..||..|...||:.:|..:|.
803    Human     3 LQVSDYSWQQTKTAVFLSLPLKGVCVRDTDVFCTENYLKVNFPPFLFEAFLYAPIDDESSKAKIG 67

804

805      Fly    62 KNEARIVLVKKEKGLW--------PEMFQKLDKEALMQ--------------KR------LEI 96
806                .:......|.|||..:|            .||.|::.::::|              ||       |.:
807    Human    68 NDTIVFTLYKKEAAMWETLSVTGVDKEMMQRIREKSILQAQERAKEATEAKAAAKREDQKYALSV 132

808

809      Fly    97 ADLIVERNKKRDE-----------KALERY-DNKRRAEIQKEIQRETDMRERVKQFQENSVREAL 149
810                ...|.|..:|:.|            ||||.: :.:|:||.||:||||..:.::.||.:|.
811    Human   133 MMKIEEEERKKIEDMKENERIKATKALEAWKEYQRKAEEQKKIQREEKLCQKEKQIKEE------ 191

812

813      Fly   150 VVDVRKEAK---ATPKPDTLQYPPSSGGASRLAT-PLMRPPMSSVRGSGRINVNFTTQHKRVTPK 210
814                ||:.|     .|....:....|....:.:.| .|....:.:.|..|.|.:|||    .||.|.
815    Human   192 ----RKKIKYKSLTRNLASRNLAPKGRNSENIFTEKLKEDSIPAPRSVGSIKINFT---PRVFPT 249

816

817      Fly   211 --RESQAAMEKAY 221
818                ||||.|.|:.:
819    Human   250 ALRESQVAEEEEW 262
820

821
```

Supplementary Figure S1. Alignment of *Drosophila* and human DNAAF4 protein sequences. Alignments were produced by DIOPT analysis. The CS domain is shown in blue. Note that evidence of conservation extends beyond the CS domain. The alignment ends at human protein residue 262, such that the C-terminal region 263-420 (which contains the TPR domain) is not present in the *Drosophila* orthologue.

Supplementary Table S1. Oligonucleotide sequences

in situ hybridisation primers

CG14921-L	TGGCCTGAGATGTTCCAGAA
CG14921-R	GTAATACGACTCACTATAGGGCCATATGCCTTCTCCATAGCGG
CG5048-L	TGGCAAGATCAGCAGGAGAA
CG5048-R	GTAATACGACTCACTATAGGGCCATAGTCTAGTTCGCGCTGC

mVenus fusion construct primers

CG14921-L	GGGGACAAGTTTGTACAAAAAAGCAGGCTGCAACCAGAGGACGCTGAATATGGATAC
CG14921-R	GGGGACCACTTTGTACAAGAAAGCTGGGTCTTCATCGACGCTCTCCATCGGCGACTG
CG5048-L	GGGGACAAGTTTGTACAAAAAAGCAGGCTCGGTGCCGTCCTTCGTCCTTT
CG5048-R	GGGGACCACTTTGTACAAGAAAGCTGGGTCAAAATTAACATAGTCTAGTT

CRISPR construct cloning

CG14921 5' sense	CTTCGTCTGCGACTGACAATAGGA
CG14921 5' antisense	AAACTCCTATTGTCAGTCGCAGAC
CG14921-L 3' sense	CTTCGTATTCATCGACGCTCTCCAT
CG14921-R 3' antisense	AAACATGGAGAGCGTCGATGAATAC

CG5048 5' sense	CTTCGTTTATGGACGGACTATCAC
CG5048 5' antisense	AAACGTGATAGTCCGTCCATAAAC
CG5048 3' sense	CTTCGTATGTCTTTTAATATTATA
CG5048 3' antisense	AAACTATAATATTAAAAGACATAC

Homology arms for CRISPR constructs

Left arm

CG14921-L	GGGGAATTCTCTGCGTACGAAATGTGCTG
CG14921-R	GGGGGTACCGGAAGGAACTTATGTTTTTGAGCTGGC

Right arm

CG14921-L	GGGAGATCTGAGAGCGTCGATGAATAAGCGTT
CG14921-R	GAACTCGAGGATCGCAGGGCACTATGTTG

Left arm

CG5048-L	CTGGAATTCCGAGCCCAAGGTGAAAGTTC
CG5048-R	GCAGGTACCCACTGGATCTCACACTTTTTC

Right arm

```
CG5048-L                      GGGAGATCTATATGGCCATTTACTTTGTG
CG5048-R                      GATCTCGAGAGGGTGTGGTTGATCATCGT
```

```
S2 Cell expression constructs
Drosophila
CG14921-L        GGGGACAAGTTTGTACAAAAAAGCAGGCTTCACCATGGTACAGATTTCGC
CG14921-R        GGGGACCACTTTGTACAAGAAAGCTGGGTATTCATCGACGCTCTCCATC
CG5048-L         GGGGACAAGTTTGTACAAAAAAGCAGGCTTCATGTCGATCTTTGACCATC
CG5048-R         GGGGACCACTTTGTACAAGAAAGCTGGGTAAAATTAACATAGTCTAGTTC
Reptin-L         GGGGACAAGTTTGTACAAAAAAGCAGGCTTCACCATGGCCGAGACCGAGAAAATC
Reptin-R         GGGGACCACTTTGTACAAGAAAGCTGGGTGTGCTCCATGGGCTGGGCATCTCCT
Pontin-L         GGGGACAAGTTTGTACAAAAAAGCAGGCTTCACCATGAAGATCGAGGAAGTCAAG
Pontin-R         GGGGACCACTTTGTACAAGAAAGCTGGGTCAACATAAACTTATTGTTCTTTTCG
Hsp90-L          GGGGACAAGTTTGTACAAAAAAGCAGGCTTCACCATGCCAGAAGAAGCAGAG
Hsp90-R          GGGGACCACTTTGTACAAGAAAGCTGGGTATCGACCTCCTCCATGTGGGA
Mouse
DYX1C1-L         GGGGACAAGTTTGTACAAAAAAGCAGGCTTCACCATGCCAGTGCGAGTGAGCGAGTT
DYX1C1-R         GGGGACCACTTTGTACAAGAAAGCTGGGTAGTCACGAGACTTCAGTGCCG
PIH1D3-L         GGGGACAAGTTTGTACAAAAAAGCAGGCTTCACCATGGAATCAGAAAATGCT
PIH1D3-R         GGGGACCACTTTGTACAAGAAAGCTGGGTAGGAAATATTAAAATCCAAATCCC
DYX1C1-L DTPR    GGGGACCACTTTGTACAAGAAAGCTGGGTAGAACTCAGGAAGGTCAGTGCTCAT
```

828